

---

# TARGET SPECIFIC DE NOVO DESIGN OF DRUG CANDIDATE MOLECULES WITH GRAPH TRANSFORMER-BASED GENERATIVE ADVERSARIAL NETWORKS

---

Atabey Ünlü<sup>1,2</sup>, Elif Çevrim<sup>1,2</sup>, Ahmet Sarıgün<sup>3,4</sup>, Melih Gökay Yiğit<sup>1,5</sup>, Hayriye Çelikkbilek<sup>1</sup>, Osman Bayram<sup>6</sup>, Heval Ataş Güvenilir<sup>1,7</sup>, Altay Koyaş<sup>7</sup>, Deniz Cansen Kahraman<sup>7</sup>, Abdurrahman Olğaç<sup>8,9</sup>, Ahmet Rifaioğlu<sup>10,11</sup>, Erden Banoğlu<sup>8</sup>, and Tunca Doğan<sup>1,2\*</sup>

<sup>1</sup>*Biological Data Science Lab, Dept. of Computer Engineering, Hacettepe University*

<sup>2</sup>*Dept. of Bioinformatics, Graduate School of Health Sciences, Hacettepe University*

<sup>3</sup>*Dept. of Chemistry, Middle East Technical University*

<sup>4</sup>*Dept. of Physics, Middle East Technical University*

<sup>5</sup>*Dept. of Computer Engineering, Middle East Technical University*

<sup>6</sup>*Dept. Of Artificial Intelligence Engineering, Bahcesehir University*

<sup>7</sup>*Cancer Systems Biology Lab, Graduate School of Informatics, Middle East Technical University*

<sup>8</sup>*Dept. of Pharmaceutical Chemistry, Faculty of Pharmacy, Gazi University*

<sup>9</sup>*Laboratory of Molecular Modeling, Evias Pharmaceutical R&D Ltd.*

<sup>10</sup>*Dept. of Electrical and Electronics Engineering, İskenderun Technical University*

<sup>11</sup>*Institute for Computational Biomedicine, Heidelberg University*

## ABSTRACT

Discovering novel drug candidate molecules is one of the most fundamental and critical steps in drug development. Generative deep learning models, which create synthetic data given a probability distribution, offer a high potential for designing de novo molecules. However, for them to be useful in real-life drug development pipelines, these models should be able to design drug-like and target-centric molecules. In this study, we propose an end-to-end generative system, DrugGEN, for the de novo design of drug candidate molecules that interact with intended target proteins. The proposed method represents molecules as graphs and processes them via a generative adversarial network comprising graph transformer layers. The system is trained using a large dataset of drug-like compounds and target-specific bioactive molecules to design effective inhibitory molecules against the AKT1 protein, which is critically important in developing treatments for various types of cancer. We conducted molecular docking and dynamics to assess the target-centric generation performance of the model, as well as attention score visualisation to examine model interpretability. Results indicate that our de novo molecules have a high potential for interacting with the AKT1 protein at the level of its native ligands. Using the open-access DrugGEN codebase, it is possible to easily train models for other druggable proteins, given a dataset of experimentally known bioactive molecules.

---

\*Corresponding author email address: tuncadogan@gmail.com

## 1 Introduction

The development of a new drug is a long-term and costly process. It entails the identification of bioactive compounds against predefined biomolecular targets as one of its initial and most essential steps. Advancements in high-throughput screening technologies now enable the simultaneous screening of tens of thousands of compounds. However, it is still impossible to analyse the entire chemical and target spaces due to their huge sizes [1], which usually prevents the discovery of the best candidate molecules. The majority of “non-ideal” drug candidates are discontinued in the late stages of the development process, such as clinical trials, due to high toxicity or low efficacy, which is the primary reason for the low success rates lately observed in drug development [2].

Small-molecule drugs developed so far exhibit low levels of structural diversity and can only target certain protein families [3]. It is possible to argue that a similar diversity problem is also valid for large virtual chemical libraries. Thus, there is a need for truly novel, i.e. structurally diverse, small molecule drug candidates to target druggable proteins in the human proteome, including their clinically significant variants [4]. Within the vast theoretical space of small molecules, estimated to be between  $10^{30}$  and  $10^{60}$  [5], compounds that have the potential to interact specifically and effectively with each targetable biomolecule may exist. The main challenge is identifying the correct molecular structures within this unexplored territory. An approach called “de novo drug design” is utilised for this. Its purpose is to design truly novel candidate molecules that are not mere derivatives of previously established molecular structures, especially to overcome hard-to-target biomolecules [6].

To address problems associated with conventional de novo drug design, such as long development durations, elevated costs, and a high number of unknown variables regarding the efficacy and safety of the designed compounds, artificial intelligence (AI) driven methods (e.g., deep generative modelling/AI) are starting to emerge in the field [7, 8, 9, 10, 11, 12, 13, 14, 15, 16, 17]. A short review of this topic can be found in the Supplementary Material (S1). Most of the methods developed so far focused on designing valid molecules that are typically small in terms of molecular size (via training the models on datasets such as QM9 (~ 9 heavy atoms on average) [18, 19] and ZINC250K (~ 23 heavy atoms on average) [8], which is an easier task compared to designing molecules that have the same size distribution as the existing drugs and bioactive molecules (29 heavy atoms in ChEMBL molecules, on average).

Deep generative models have also been used to design molecules with desired properties via conditioning the training or the prediction procedure(s). Most of these models have utilised condition vectors as a tool for property injection into the generative process. VAEs [20, 21, 22], GANs [10, 23, 24], sequence-based (language) models [25, 26, 27, 28], geometric models [29] and diffusion models [15, 30] have been utilised for conditional molecule generation tasks. Reinforcement learning (RL) has also been employed for this purpose, with reward-penalty functions guiding models towards desired molecular characteristics in the respective latent space [27, 31]. These approaches result in optimised molecule generation; however, one of the fundamental objectives of drug design is developing small molecules that will physically interact with the desired target, and obtaining de novo molecules with optimised properties alone is insufficient to satisfy this goal. Although a few recent studies present prototype models [32, 33, 34, 35, 36, 37, 38, 39], AI-driven target-centric drug design is a highly novel and understudied area with great potential to contribute to rational drug design.

In this study, we propose DrugGEN, a new de novo small molecule design system, an end-to-end framework, that generates target-centric drug-like molecules using the GAN and transformer architectures [40], incorporating graph representation learning [41]. The workflow of the study is depicted in Figure 1. The process (i) starts with the preparation of small molecule datasets (including their bioactivities/interactions) and their encoding as graphs to be used as training and test data (Figure 1A), (ii) proceeds with the design and implementation of the DrugGEN model together with the training and evaluation of the system in the context of performance comparison with the state-of-the-art and an ablation study (Figure 1B), and (iii) concludes with the downstream analysis of generated molecules and selection of the most promising candidates to effectively target the selected protein (Figure 1C). In item iii, we generated and evaluated novel inhibitors for the “RAC-alpha serine/threonine-protein kinase” (AKT1) protein (Figure S1). Additional information about AKT1 is provided in Supplementary Material (S2).

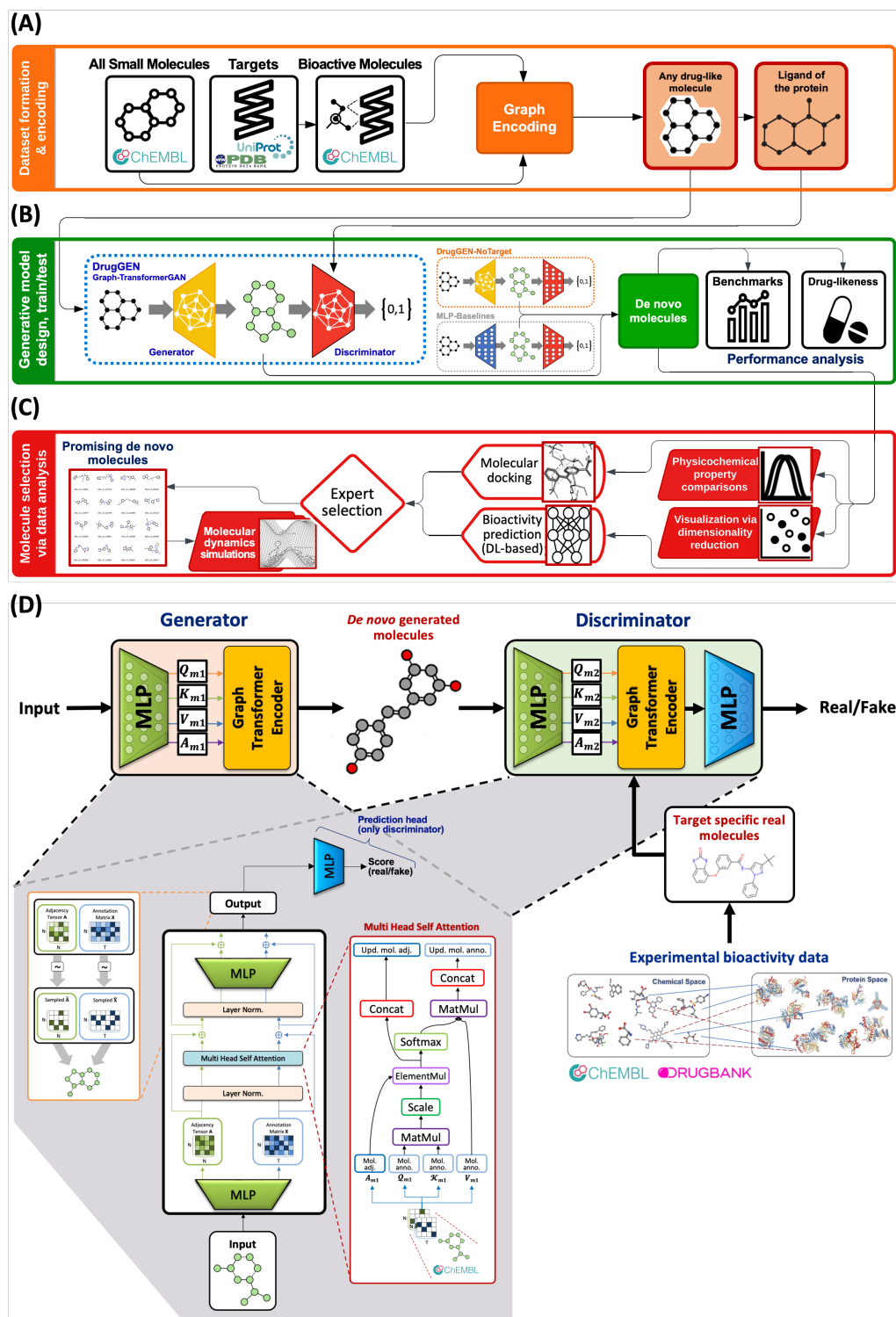


**Figure 1:** The workflow of the study. **(A)** Preparation of datasets including molecules and bioactivities, together with the graph-based encoding of samples in datasets, **(B)** the graph transformer GAN-based architecture of DrugGEN, model training and evaluation via subjecting de novo molecules to fundamental benchmarks and drug-likeness-related metrics, and **(C)** subsequent selection of molecules via a series of in silico experiments to identify promising candidates that effectively target the selected protein, **(D)** the schematic representation of the architecture of the DrugGEN model. The generator module of the GAN, which consists of a graph transformer encoder module, transforms the given input into a new molecular representation. The MLP-based discriminator of the GAN compares the generated de novo molecules to the known inhibitors of the given target protein, scoring them for their assignment to the classes of “real” and “fake” molecules (abbreviations; MLP: multi-layered perceptron, Norm: normalisation, Concat: concatenation, MatMul: matrix multiplication, ElementMul: element-wise multiplication, Mol. adj: molecule adjacency tensor, Mol. Anno: molecule annotation matrix, Upd: updated).

## 2 Results

### 2.1 The Overview of DrugGEN

DrugGEN aims to learn the distributions of physicochemical properties and topological attributes of drugs and drug candidate molecules from the given data to generate drug-like small molecules that are valid and novel. The discriminator network takes the de novo molecules designed by the generator and compares them with the known (real) bioactive ligands (inhibitors) of the selected target protein so that the differences (in terms of structural properties) between the de novo and real molecules can be learned by the model. This information is then shared with the generator network in an adversarial setting. This approach directs the generation process toward ligands interacting with the selected target. The main technical novelty in the DrugGEN model is the incorporation of graph transformers into the generator and discriminator modules of the generative adversarial network (GAN) (Figure 1D), the aim of which was to overcome problems related to handling the complexity of the target-centric generation process, especially considering the large sizes of drug-like molecules, by effectively learning the long-range dependencies between the atoms of small molecules, and overall, their interactions.

DrugGEN is trained with small molecule data, including random drug-like small molecules and known target-specific inhibitors (from ChEMBL and DrugBank databases), and applied for designing de novo ligands of the "RAC-alpha serine/threonine-protein kinase" (AKT1) protein. Its effectiveness was assessed through a series of downstream data analyses (Figure 1B and C). The performance of DrugGEN was evaluated via known benchmarking metrics. DrugGEN's molecules were also explored in comparison to real molecules via (i) physicochemical property value distribution plots and (ii) UMAP / t-SNE projections and visualisation in 2-D. Additionally, target-centric properties of the generated molecules were evaluated further via *in silico* experiments, such as molecular docking and deep learning-based drug-target interaction prediction. In our tests, we also compared DrugGEN with other generative models. Furthermore, we conducted an explainable AI-centric analysis via attention score visualisation to interpret the model. We selected 30 promising candidate de novo molecules via expert curation. Finally, we performed molecular dynamics simulations with (i) the native ligand in the co-crystal structure of AKT1 (PDB id: "4GV1") [42], and (ii) a chosen de novo generated molecule to compare their binding characteristics within the AKT1 binding site. Each of these analyses is described in detail in the subsequent sections.

### 2.2 Performance Evaluation and Comparison

We compared DrugGEN's performance with methods from the molecular generative AI literature. For this, we generated 10,000 de novo molecules (using our trained model in the inference mode) and subjected these molecules to MOSES benchmarking [43]. Here, we report the generative performance of DrugGEN and other models using the widely known metrics of validity, uniqueness, novelty, internal diversity (IntDiv), and quantitative estimate of drug-likeness (QED) where higher values indicate better performance (see "Performance metrics" in Methods for details). It is important to note that these benchmarking metrics only provide clues about the performance of a generative model on a basic level. They do not offer a comprehensive evaluation, which is a difficult task since the main aims of these models are different from each other (e.g., designing a valid molecule, optimising molecules over a physicochemical property, etc.). Target-specific molecule generation, which is the main goal of DrugGEN, cannot be assessed by these metrics; therefore, this property has been evaluated at later steps via physics-based analyses such as molecular docking and dynamics.

In Table 1, DrugGEN's performance is shown together with other models from the literature (i.e., ORGAN, MolGPT, MGM, RELATION, REINVENT, MARS, BIMODAL, molDQN, QADD, STAGAN, ResGen and EDM). The competing models were selected based on the underlying algorithms and training datasets to cover a wide range of approaches. Since this analysis has multiple metrics and numerous methods, it was not straightforward to make a generalised comparison. To solve this issue, we calculated an overall ranking by considering all the metrics together (where rank 1 is the best). For this, we divided the methods into three groups: the best, medium and low, and scored them with 1, 2 and 3, respectively, independently for each metric. The methods are ranked from lowest to highest average score. DrugGEN became the top model in the overall ranking.

Considering individual metrics, DrugGEN displayed a high performance on most of them and did not suffer from issues such as low validity, novelty or uniqueness, which is the opposite of ORGAN, BIMODAL, REINVENT, MGM and ResGen. Of these models, ORGAN relies on the GAN structure composed of an RNN (as a generator) and a CNN (as a discriminator) to generate conditioned molecules [44]. Another GAN-based model, STAGAN, was introduced to mitigate mode collapse observed in conventional GANs. Nevertheless, the model exhibits diminished validity, particularly when confronted with the challenge of processing considerably larger molecular structures within the ZINC250k dataset ( 23 heavy atoms on average) [11]. On the other hand, DrugGEN utilises graph transformers with attention modules, which might contribute to the performance difference.

**Table 1:** Molecule generation performance of DrugGEN and other methods: RELATION [38],MGM [12], MolGPT [26], ORGAN [44], QADD [45], molDQN [46], BIMODAL [47], MARS [48], REINVENT [49], ResGen [29], EDM [15], and STAGAN [11] were given in terms of fundamental benchmarking metrics of internal diversity (IntDiv), novelty, validity and uniqueness (Uniq.). We directly obtained the scores from the articles of these models, except for the EDM, for which we re-trained the model with the ChEMBL dataset, and ResGen, for which we used the trained model to generate molecules and calculate metrics. The ORGAN and STAGAN models are trained on a curated ZINC dataset, whereas the RELATION and MolDQN models utilise a combination of ChEMBL and ZINC data for training. The remaining models are trained exclusively on the ChEMBL data. Arrows show the direction in which the performance increases. The best performances are displayed in bold font (all within %1 of the highest score).

Data Type	Model Name	Architecture details	Validity (↑)	Uniqueness (↑)	Novelty (↑)	IntDiv (↑)	QED (↑)	Overall ranking (↓)
Text	REINVENT	RNN + RL	0.940	0.307	-	0.755	0.525	6
	BIMODAL	RNN	0.997	0.314	-	0.720	0.541	6
	RELATION	BiTL	0.854	<b>1.000</b>	<b>1.000</b>	0.773	-	3
	MolGPT	Transformer	0.994	0.797	<b>1.000</b>	0.857	-	2
	ORGAN	GAN	0.379	0.687	0.841	-	0.520	8
Graph	QADD	GNN + RL	<b>1.000</b>	0.341	-	0.613	-	9
	MARS	GNN + MCMC	0.997	0.333	-	0.641	-	9
	MGM	MPNN	0.849	0.722	<b>1.000</b>	-	<b>0.582</b>	3
	molDQN	Q-Learning (RL)	<b>1.000</b>	0.360	-	0.531	-	9
	STAGAN	GAN	0.482	<b>1.000</b>	1.000	-	-	5
	ResGen	GVP	-	<b>1.000</b>	0.289	0.547	0.218	12
	DrugGEN (ours)	GAN + Graph transformer	0.931	<b>0.991</b>	<b>1.000</b>	<b>0.875</b>	0.520	1

\*RNN: Recurrent Neural Networks, RL: Reinforcement Learning, BiTL: Bidirectional Transfer Learning, GAN: Generative Adversarial Networks, GNN: Graph Neural Networks, MCMC: Markov chain Monte Carlo, MPNN: Message-passing Neural Networks, GVP: Geometric Vector Perceptron.

The MolGPT model employs the conventional sequence-based transformer architecture utilised in natural language processing. This model was trained using SMILES representations of molecules. However, the novelty score of the model was reported to be subpar. Furthermore, models such as QADD, molDQN, BIMODAL, REINVENT, and MARS also exhibit low novelty scores caused by generating existing samples in the training set. On the contrary, DrugGEN generates a significantly higher rate of novel molecules (Table 1). We also calculated the average maximum and mean pairwise Tanimoto-based similarity values between DrugGEN’s de novo molecules and all real molecules in the ChEMBL dataset and found 55% and 11% similarity, respectively, which points to the high originality of DrugGEN molecules. The internal diversity (IntDiv) metric indicates the diversity of structures among generated samples. DrugGEN also exhibited notably high performance in IntDiv, demonstrating its ability to learn different molecular structures from the training dataset. Additional comments can be found in Supplementary Material (S3).

## 2.3 Ablation Study

In this analysis, we compare the output of different DrugGEN model variations with each other and with the molecules in the training datasets. We used the same set of fundamental benchmarking metrics as in the previous section, as well as the synthetic accessibility (SA) metric [43] (see “Performance metrics” for details). For this experiment, we utilised four different models: (i) DrugGEN: the default model, (ii) DrugGEN-NoTarget: a DrugGEN model that only generates random molecules, which has the same architecture as DrugGEN; however, its discriminator takes random real molecules as input instead of target specific inhibitors (the sole aim is to generate drug-like molecules), (iii) MLP baseline: a targeted baseline model with multi-layered perceptron (MLP) based generator/discriminator modules, and (iv) MLP-NoTarget baseline: a MLP-based non-targeted baseline model. These baseline models are differentiated from DrugGEN by replacing the graph transformer encoder blocks with simple MLP layers (please see “Methods” for details). The purpose behind comparing the main DrugGEN model and its non-targeted version with the MLP-based baselines is to underscore the benefits of employing graph transformers for molecule generation. Targeted and non-targeted baseline models follow the same training schedule and datasets as DrugGEN and DrugGEN-NoTarget, respectively. We generated 10,000 de novo molecules from each model and ran them through the metrics mentioned above.

Table 2 shows ablation performance results, in which all models demonstrate high validity, uniqueness, novelty, and IntDiv scores, indicating the high efficiency of our molecular design system. Low SA and high QED scores pinpoint the easy synthesizability of the generated molecules, in comparison to ChEMBL data (random drug-like molecules) and real AKT1 inhibitors. DrugGEN’s generator module takes random molecules as the initial input (i.e., starting molecules). Therefore, measuring a second novelty score against the starting molecules used during the generation process is also essential. We named this metric novelty at inference (NI) and provided the scores in Table 2 in the same column as the regular novelty measure (i.e., novelty against training data). We observed that NI scores are slightly lower than the standard novelty values, which was expected since the input of the inference run has a more direct effect on generated samples. It is also important to note that the NI scores of DrugGEN are still higher than the regular novelty scores of most of the models listed in Table 1. Meanwhile, both the DrugGEN-NoTarget and the MLP-NoTarget baseline models scored low NI values (0.552 and 0.201, respectively), indicating that these models generate their starting molecules at least half of the time. Additional comments can be found in Supplementary Material (S3).

We also docked molecules belonging to each model/dataset to the AKT1 protein structure (details are provided in Methods). The median scores (using the best 10% of molecules in terms of docking scores) are shown in the docking score column of Table 2. The results indicate that the real AKT1 inhibitors obtained the best performance (-9.406 kcal/mol), which was expected since these are experimentally verified binders and included as positive control. The DrugGEN model has obtained the closest results to real AKT1 inhibitors (-8.369 kcal/mol). On the other hand, the MLP baseline model falls short (-6.367 kcal/mol), pointing out that MLP lacks the required generalisation capability to understand long-term relationships between atoms of the molecule to design effective inhibitors. On the other hand, the transformer architecture leverages the attention mechanism to effectively extract the intrinsic structural patterns. A more detailed investigation of the docking analysis is provided below, in the “Molecular docking analysis” section.

Overall, the ablation results indicate a better targeted generation performance when the graph transformer blocks are utilised. Based on the results in Tables 1 and 2, it is possible to state that DrugGEN generates valid, diverse and novel molecules, which docks well to the intended target.

## 2.4 Physicochemical Property Comparisons

We drew histograms (density plots) displaying the physicochemical property value distributions of real molecules in our training dataset and de novo generated molecules from DrugGEN models and other target-based generation models (Figure S2). Details of this analysis are given in Supplementary Material (S4). In summary, de novo molecules belonging to the DrugGEN model and real AKT1 inhibitors share a similar region of the physicochemical property space in general (i.e., DrugGEN’s

**Table 2:** Ablation study performance results in terms of (i) fundamental benchmarking metrics (i.e., validity, novelty, uniqueness, and IntDiv), (ii) metrics measuring physicochemical and drug-likeness-related properties (i.e., QED, and SA), and (iii) docking scores (kcal/mol) obtained against the AKT1 protein structure (i.e., median of the scores of the top 10% of molecules). Arrows show the direction in which the performance increases.

Models/ Datasets	Highlight of the Model/Dataset	Validity (↑)	Novelty (NI*) (↑)	Uniqueness (↑)	IntDiv (↑)	QED (↑)	SA (↓)	Docking score (↓)
ChEMBL Data	Training data (random mol.*)	-	-	-	0.877	0.543	3.002	-6.871
Real AKT1 Inhibitors	Training data (targeted mol.)	-	-	-	0.827	0.460	3.051	-9.406
DrugGEN	Targeted gen. via graph trans.	0.931	0.991 (0.949)	1.000	0.875	0.520	2.842	-8.369
MLP Baseline	Targeted gen. via MLPs	0.934	0.992 (0.952)	1.000	0.860	0.519	2.833	-6.367
DrugGEN NoTarget	Non-targeted gen. via graph trans.	0.913	0.990 (0.552)	1.000	0.884	0.578	3.030	-
MLP-NoTarget Baseline	Non-targeted gen. via MLPs	0.957	0.999 (0.201)	0.998	0.883	0.576	2.821	-

\*mol: molecules, NI: Novelty at Inference (novelty measured against the real molecules used as input at inference), MLP: multi-layered perceptron.

distribution shape and mean more closely resemble those of real AKT1 inhibitors compared to other models). This finding indicates that DrugGEN has effectively learned the physicochemical properties of the real inhibitors of the selected target protein. It is also important to note that this correlation is not due to merely overfitting to the training dataset, indicated by the high novelty scores (Table 1 and 2).

## 2.5 Molecular Docking of de novo Molecules

To examine target-centric binding characteristics of de novo generated molecules, we conducted a molecular docking analysis (please see “Methods” for details) on the de novo molecules generated by DrugGEN and competing targeted molecule generation methods (i.e., RELATION, TRIOMPHE-BOA, and ResGen). We also employed the real AKT1 inhibitors as the positive control, and baselines (i.e., DrugGEN-NoTarget, MLP, MLP-NoTarget, and randomly selected ChEMBL molecules) as the negative control. We utilised the AKT1 crystal structure (PDB id of the model: “4GV1”)[42] as our template. Figure 2A displays bar plots of median docking scores (i.e., binding free energies -  $\delta G$  in kcal/mol) of the top 10% of molecules with the best binding properties from each group/model, where a lower binding free energy value indicates a stronger binding affinity. Predicted binding free energies for all molecules are given as histograms in Figure S3. The median docking scores of DrugGEN and positive/negative controls were already provided as part of the ablation study, above (Table 2).

In Figure 2A, percentages shown on top of each bar represent docking performance of generative models in comparison to the real AKT1 inhibitors. For this, we applied min-max normalisation to the median docking score of each model (parameters: maximum=-9.41 and minimum=-3.75 kcal/mol, which are the median of the top and bottom 10% docking scores of real AKT1 inhibitors, respectively). DrugGEN achieved the highest performance with 81.64% and -8.37 kcal/mol (Figure 2A), exhibiting a noteworthy contrast to other target-based models, especially TRIOMPHE-BOA, and ResGen, as well as the non-targeted model, DrugGEN-NoTarget. Furthermore, the difference between the DrugGEN and RELATION models (i.e., -8.37 and -8.10 kcal/mol, respectively) was found to be statistically significant according to the Mann-Whitney U rank test (p-value < 0.0001). Additionally, we measured the docking binding free energy of the capivasertib-AKT1 complex (i.e., the bound ligand in our template PDB structure: 4GV1) at -9.52 kcal/mol, as well as other

experimentally proven inhibitors that reached clinical trials, namely ipatasertib and uposertib, at -9.68 and -8.57 kcal/mol, respectively. The DrugGEN model was able to generate 38 molecules that surpass the binding score of the native ligand capivasertib, which are shown in Figure S4.

As an overall evaluation, DrugGEN was successful in its target-specific molecular design routine. After this stage of the study, we concentrated on further investigating DrugGEN's de novo molecules and selecting a subset to propose as new potential inhibitors for AKT1.

## 2.6 Exploration of Molecules via Dimensionality Reduction

We visualized both real and de novo molecules from the previous analyses using UMAP [50] and t-SNE [51] algorithms. Figure 2B and C present the UMAP (parameters: n-neighbors=50, min-dist=0.8 and metric="dice") and t-SNE (parameters: perplexity: 500, iteration: 2000) projections, respectively, of a randomly selected subset of de novo molecules from DrugGEN and DrugGEN-NoTarget models (1,000 from each), real AKT1 inhibitors (all molecules used in model training); and 50,000 ChEMBL molecules from the training dataset. In these plots, each dot represents a molecule, colours indicate their source, and the Euclidean distances roughly indicate structural similarities based on Tanimoto applied on descriptor-based molecular fingerprints. The molecules are represented by the MACCS (Molecular ACCess System) descriptors, which is a 166-D set of binary fingerprints concerning the presence or absence of predefined structural features [52].

In the UMAP and t-SNE plots in Figure 2B and C, molecules generated by the DrugGEN model are clustered together with real AKT1 inhibitors, indicating a higher structural resemblance (in terms of topological fingerprint-based similarities). On the other hand, molecules generated by DrugGEN-NoTarget exhibit a nearly homogeneous distribution across the entire plane, due to the non-targeted generation approach. Our conclusion here is that the DrugGEN model has learned the structural distribution of the AKT1 inhibitor molecules.

## 2.7 Analysing Molecules with Drug-likeness Filters

To assess their drug-related properties, de novo molecules generated by DrugGEN are subjected to the following filtering steps: (i) Lipinski's Rule of 5 [53], (ii) Veber's rules [54], and (iii) the pan-assay INterference compoundS (PAINS) [55] filter, which identifies and eliminates false positive molecules in biological screening assays such as redox cyclers, toxoflavins, polyhydroxylated natural phytochemicals, etc. In this analysis, we utilised the same 10,000 de novo generated molecules subjected to the benchmarking analysis. In the end, 41.15% (4,115 out of 10,000) of the de novo molecules successfully passed through the filters. Subsequently, we subjected ChEMBL and AKT1 molecules to the same filters for comparison. It is observed that 57.18% (1,342 out of 2,347) of AKT1 inhibitors and 50.80% (50,802 out of 100,000) of randomly sampled ChEMBL dataset molecules have passed, providing roughly similar percentages to DrugGEN molecules.

## 2.8 Deep Learning-based Bioactivity Prediction

To evaluate the target interaction-related properties of de novo molecules in parallel to molecular docking, we carried out a deep learning-based drug/compound-target interaction (DTI) prediction analysis with the same de novo molecule dataset (against the AKT1 protein), using our previously developed DEEPScreen system [56]. DEEPScreen is a supervised discriminative deep learning system composed of target-centric bioactivity prediction models that classify input molecules as either active (interacting) or inactive (noninteracting) against the selected protein (Figure 2D) (please see "Methods" for details). We preferred DEEPScreen for this analysis since (i) it is straightforward to prepare input data and train/test a target-specific DTI prediction model, (ii) it only requires readily available data, (iii) it has high predictive performance as displayed in its respective article [56]. DEEPScreen is completely separate/ independent from the DrugGEN system regarding the modelling approach, datasets and output. Therefore, it is ensured that the DTI prediction analysis is objective. Out of 10,000 molecules obtained from the DrugGEN model, DEEPScreen predicted

5,700 of them as active, and 373 of these active predictions received an extraordinary confidence score of  $\geq 0.85$  (the complete confidence score histogram of the active predictions is given in Figure S5). We also analysed 2,347 real AKT1 inhibitors, 10,000 random ChEMBL compounds and 10,000 DrugGEN-NoTarget molecules with DEEPScreen for comparison, which received 777, 168 and 138 high confidence ( $\geq 0.85$ ) active predictions against the target protein, respectively. The high ratio of real AKT1 inhibitors can be deceiving here since most of these “active” predicted molecules were already presented in the positive training or validation datasets of the DEEPScreen model. As a result, the model was highly biased towards predicting these molecules as active. Considering the two non-targeted molecule groups (i.e., DrugGEN-NoTarget and random ChEMBL molecules), the difference in the number of high-confidence active predictions (373 vs. 168 and 138) indicates the effectiveness of DrugGEN. In accordance with the results of the docking analysis, these findings provide additional information on DrugGEN’s ability to generate target-based molecules.

## 2.9 Final Candidate Molecules Selection

We manually selected the 30 most promising de novo molecules (from molecules with docking scores  $< -8$  kcal/mol and DEEPScreen predictions as “active”) via expert curation and presented them as our best candidates to target AKT1 (Figure 3). Figure S6 shows a subset of those 30 de novo molecules alongside the real AKT1 inhibitory molecules (from the training dataset) most similar to them (two real molecules for each de novo design). As observed from Figure S6, de novo molecules are structurally diverse even from their most similar counterpart in the training set, yet these molecules obtained convincing docking scores (i.e.,  $< -8$  kcal/mol) against AKT1.

We showcase one molecule among the 25 (shown with the identifier: “*MOL\_01\_027820*” in Figure 5), which can be denoted as a “Pyrrolo[1,2-a]pyrimidin-4(1H)-one” derivative. Figure 4A displays the reference crystal complex structure of AKT1 with the ligand capivasertib (model PDB id: “4GVI”) [42], for which the binding free energy was measured as  $-9.517$  kcal/mol in the molecular docking analysis (on the same ligand conformer). Figure 4B shows the best docking pose of *MOL\_01\_027820* with the binding free energy  $-9.686$  kcal/mol obtained via the same docking protocol. This molecule is investigated further below to comprehend its binding-related dynamic properties.

## 2.10 Investigation of Binding Properties of the de novo Showcase Molecule

The reference co-crystal complex structure “AKT1 - capivasertib” (Figure 4A) and the complex model obtained from the docking of the selected de novo molecule “AKT1 - *MOL\_01\_027820*” (Figure 4B) share the binding pattern with Ala177, Lys179 and Thr291. Hydrophobic interactions are more prominent in the AKT1 - *MOL\_01\_027820* complex, whereas in the crystal structure hydrogen bonds are evident. This may contribute to the difference in binding affinities. The replacement of the adenine ring of the ATP with various heterocyclic moieties resulted in selective and potent inhibition of kinases and this mode of binding constitutes more than 90% of kinase inhibitors [57]. These inhibitors bind the same binding pocket as ATP and mimic adenine group’s interactions with the hinge residues. Here we see a similar orientation with capivasertib and *MOL\_01\_027820* in the AKT1 kinase binding site. However, the hydrogen bond interactions with the backbones of the hinge residues were not directly observed in the docking-derived binding pose of *MOL\_01\_027820* (Figure 4B). To further evaluate the relaxation and adaptation of the binding site and to reveal binding characteristics of capivasertib and *MOL\_01\_027820*, 500 ns long molecular dynamics (MD) simulations were conducted with four copies (please see “Methods” for details).

The output of MD simulations are shown in Figure 4 panels C to I. The AKT1 structure mostly consists of  $\alpha$  helices, and visual inspection of the simulations displayed the conservation of secondary structures during the simulations of both complexes. As can be seen in RMSD plots (Figure 4 panels F to I), both simulations (together with their simulation copies) reached stable binding patterns. Hydrogen bonding networks between the hinge domain residues Glu228 and Ala230 occurred with high ratios in all simulations. Van der Waals interactions were also observed with the hydrophobic moieties of the surrounding residues. The gatekeeper residue Met227 remained closed and supported the residence of the ligand within the binding cavity for both complexes. Additionally, Lys179 in

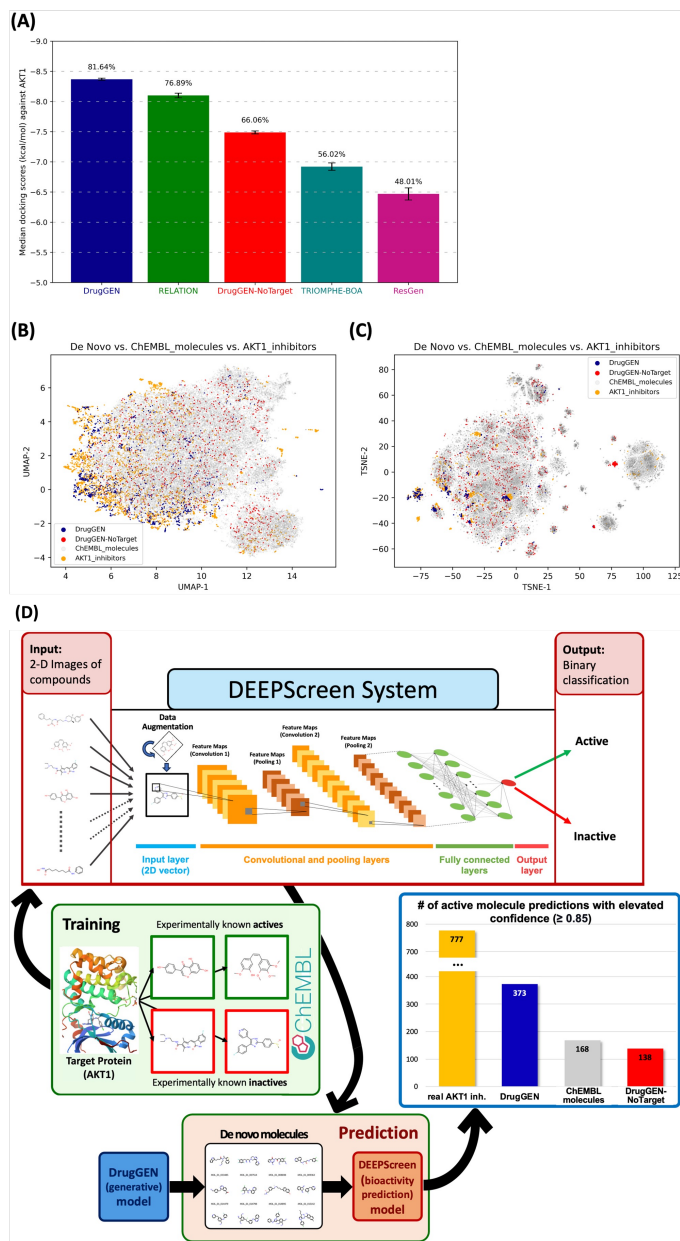


**Figure 2:** Exploration of de novo molecules via downstream analysis. (A) Bar plots displaying the median of binding free energies measured in the docking analysis of de novo molecules generated by DrugGEN, DrugGEN-NoTarget, RELATION, TRIOMPHE-BOA, and ResGen models (molecules are docked into the binding pocket of the AKT1 protein structure). The whiskers on the bars represent the standard error of the median (median values are utilised due to the non-normal distribution of data). The percentages given above each bar represent docking scores normalised with respect to the scores of real AKT1 inhibitors, with the top real AKT1 inhibitors set at 100%. (B-C) 2-D visualisation of the molecules generated by DrugGEN and DrugGEN-NoTarget models, real AKT1 inhibitors and randomly selected ChEMBL molecules via UMAP (B) and t-SNE (C) projections. (D) Deep learning-based bioactivity prediction analysis. Top: the work-flow of DEEPScreen, which uses 2-D pixel-based (image) structural representations of molecules as input and processes them via deep convolutional neural networks [56]. Middle: the DEEPScreen AKT1 model is trained with binarised experimental bioactivity data points of the AKT1 protein (obtained from ChEMBL binding assays) and subjected to DrugGEN's de novo molecules in the inference/prediction mode. Right: bioactivity prediction results, i.e., the number of high-confidence active predictions among the real AKT1 inhibitors, randomly selected ChEMBL molecules, and DrugGEN and DrugGEN-NoTarget molecules.

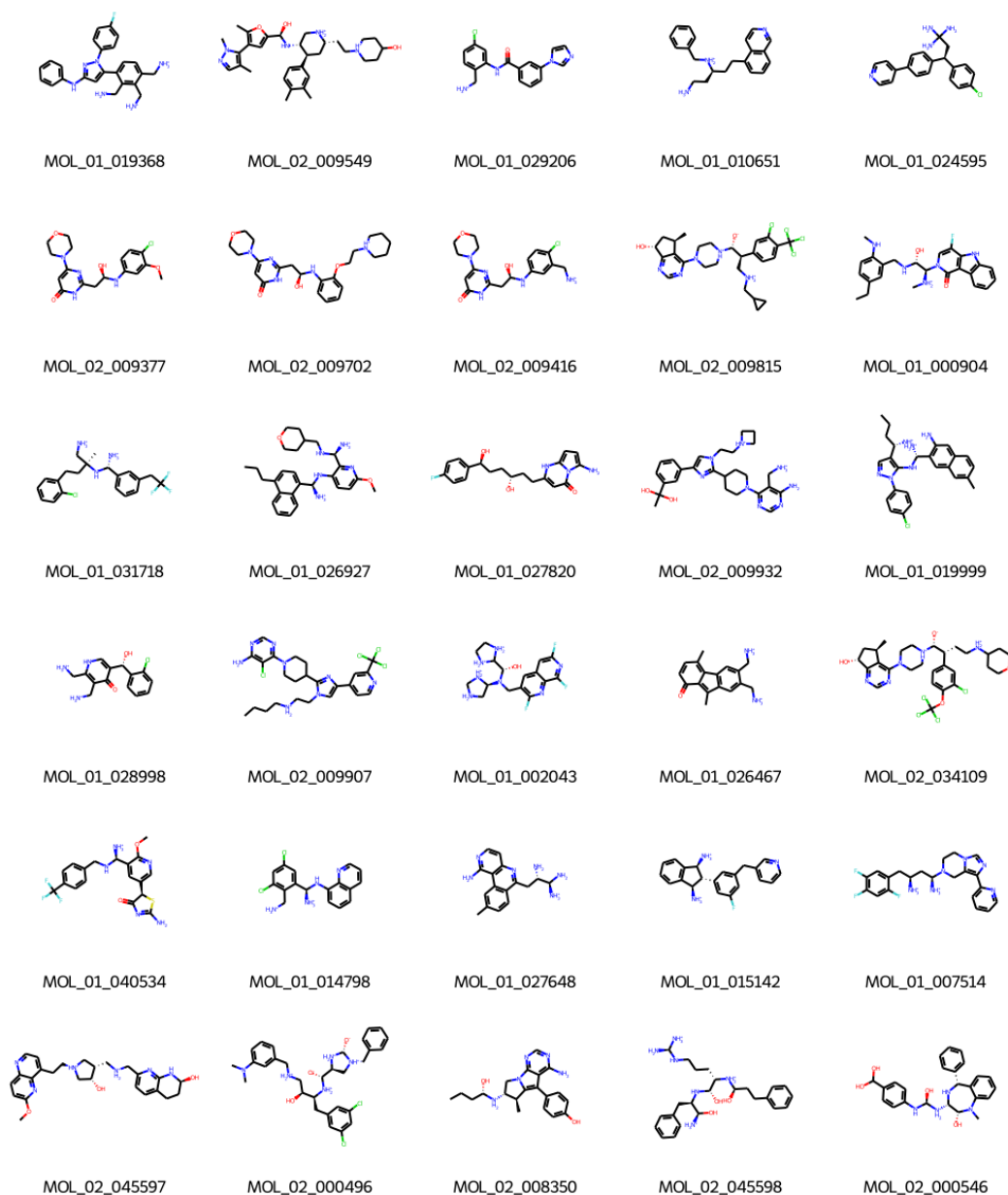


**Figure 3:** 30 promising de novo molecules to effectively target AKT1 protein (generated by DrugGEN model), selected via expert curation from the dataset of molecules with sufficiently low binding free energies ( $< -8$  kcal/mol) in the molecular docking experiment and deep learning-based DTI predictions (by DEEPScreen [56]) as “active”.

$\beta$ -sheet continued to form a salt bridge with Glu234 in the  $\alpha$ C-helix located at the N terminal domain of AKT1. This was a supporting factor to keep the ligand within the binding site. With the help of this ionic interaction, the protein stayed in DFG-in and  $\alpha$ C-helix in conformation in the simulations.

Capivasertib remained stable during all simulations (RMSD  $< 1$ , Figure 4 panels F and H). The interaction analysis of capivasertib showed that hydrogen bonds with the hinge domain (via Glu228 -99%- and Ala230 -99%- residues) were conserved during the simulation. An additional hydrogen bond was seen with Glu278 (74%). *MOL\_01\_027820* showed two different binding patterns

(pattern-1 and -2, shown in Figure 4 panels D and E, respectively). Those patterns were seen in two individual copies of the simulations. Pattern-1 was observed in the second and the third replica simulations and pattern-2 was observed in the first and the fourth replicas (Figure 4G). The first pattern was similar to the docking-derived starting conformation ( $RMSD_{average} = 1.2$ , Figure 4 panels D, G, and I) and relatively close to the binding pattern with the compound capivasertib. However, the second pattern showed 110.2 degrees of dihedral tilting ( $RMSD_{average} = 3.1$ , Figure 4 panels E, and G) following atom number 15 and above (Figure 4I) but still conserved the essential interactions with the hinge domain and remained within the binding cleft and conserved the protein's general conformation. Further comments can be found in Supplementary Material (S5).

In summary, we found that the binding features of capivasertib and the conformations of AKT-1 were conserved during the simulations. The simulation analysis results of *MOL\_01\_027820* revealed two different binding patterns. Still, they kept the molecule within the binding cleft, conserved the interactions within the adenine region and conserved the protein's general DFG-in and  $\alpha$ C chain-in conformation. This indicates that DrugGEN was able to learn the binding features of the target protein (Figure 4).

## 2.11 Attention map visualisation

Artificial neural networks are generally characterised as black box models that lack interpretability. On the other hand, transformer-based models weigh intrinsic pairwise relationships between data tokens through the attention mechanism, which can be utilised to visualise the important relationships in the data and, therefore, interpret what the model learns. Adopting this strategy, we visualised the average attention scores (produced by the transformer encoder module of the generator network) for each atom in the selected de novo generated molecules to assess critical atoms and bonds according to the model's perspective. We observed the correspondence between the atoms that received high attention scores and those interacting with AKT1 protein's binding pocket residues according to the molecular docking analysis (Figure 5 and Figure S7). A high correspondence would indicate that the model learned which atoms are critical for enabling physical interaction with the target.

In Figure 5, interactions between the atoms of de novo molecules and residues in the AKT1 binding pocket are visualised via 2-D protein-ligand interaction diagrams for three different de novo molecules (Figure 5A, C, and E), using a 4 Angstrom cutoff. Also, in Figure 5, the same de novo molecules' atoms with the highest average attention scores are visualised with green, yellow and red, indicating the importance appointed by the model (Figure 5B, D, and F). The de novo molecules employed in this analysis were randomly selected from the 30 promising molecules given in Figure 3.

Considering all three cases in Figure 5, the model identifies most of the atoms interacting with the target residues by assigning high attention scores. For example, in Figure 5A and B, N+H atoms forming both salt bridges and hydrogen bonds with the residue Glu234, and HN and N atoms forming hydrogen bonds with the residues Asp274 and Ala230, respectively, are assigned the highest attention values (i.e., the green coloured ligand atoms). The same pattern is observed for other interactions in Figure 5. Overall, 20 out of 22 (91%) ligand atoms in pairwise interactions were detected by the generator network of DrugGEN. Looking at the same examples from the other angle, 20 out of 24 (83%) ligand atoms with top attention scores were in contact with the target residues, thus playing a critical role in the interaction. Even though the model did not use any data regarding pairwise molecular interactions during training and validation, it still managed to learn substructures crucial for binding to AKT1 and designed molecules accordingly. These findings illustrate the utility of attention maps to understand the model's generative process. We provided two additional examples in Figure S7 with a similar outcome.

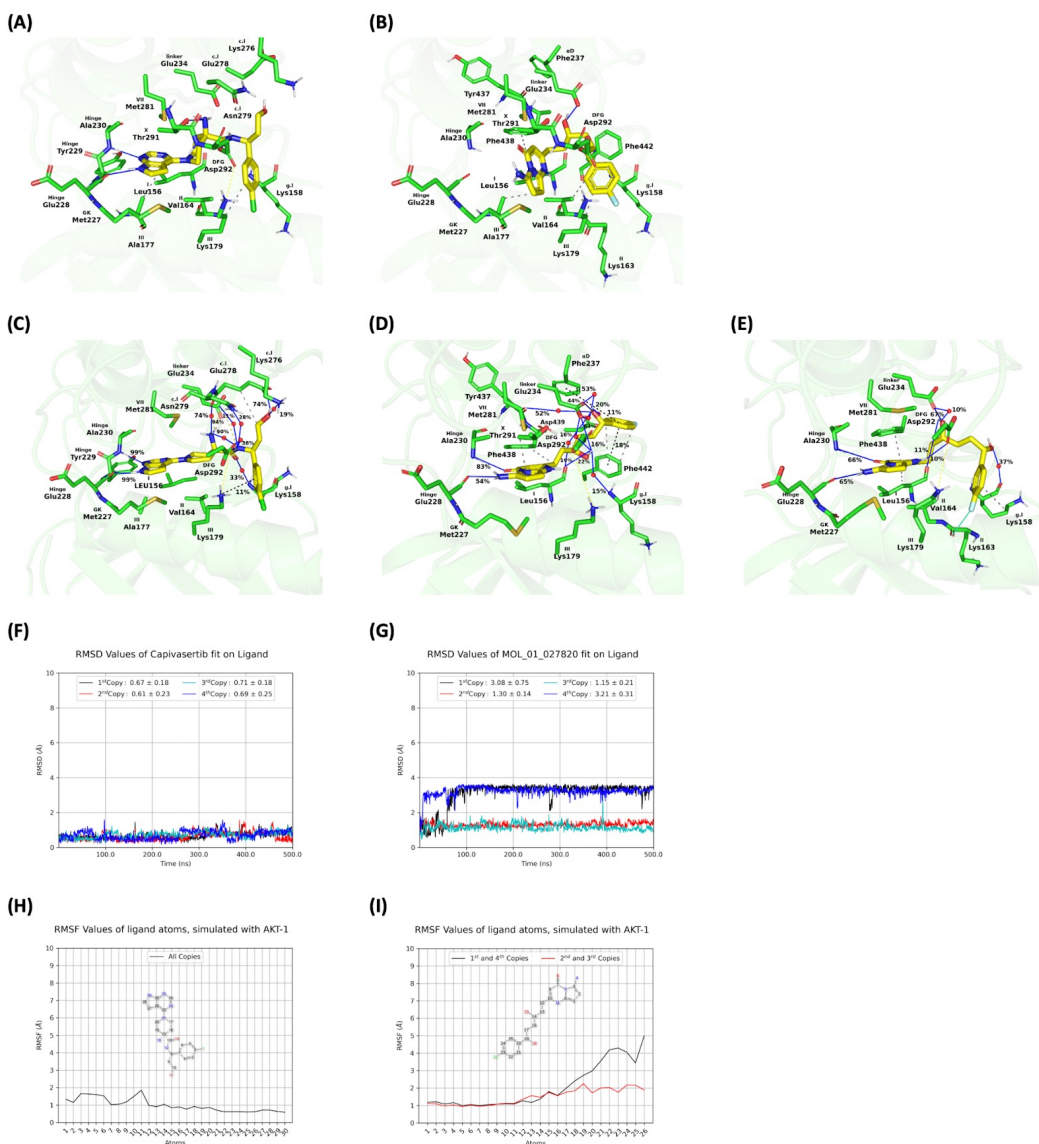


**Figure 4:** The output of the structural analysis of selected molecules: Capiwasertib (the ligand from the crystal structure PDB id: “4GV1”) [42] and the showcase de novo generated molecule: “Pyrrolo[1,2-a]pyrimidin-4(1H)-one” derivative (*MOL\_01\_027820* in Figure 3). Block I: Molecular docking results: (A) AKT1 crystal complex structure with the co-crystallized ligand: Capiwasertib (binding free energy in docking: -9.517 kcal/mol), and (B) The best pose in the molecular docking of the showcase de novo generated molecule *MOL\_01\_027820*, to the structurally resolved binding site of AKT1 (binding free energy in docking: -9.686 kcal/mol). Gray dashed lines represent Van der Waals interactions. Blue lines represent hydrogen bonds. Yellow dashed lines represent salt bridges. Block II: The molecular dynamics simulation output. The occupancy values of: (C) the single binding pattern of capivasertib, (D) the first binding pattern of *MOL\_01\_027820*, and (E) the second binding pattern of *MOL\_01\_027820* in complex with AKT1 obtained from the MD simulations. Noninteracting backbone atoms are hidden for visual clarity. Only the interactions above 10% occupancy values are reported. Domain names are noted on the figure as given in the KLIFS database [58]. Abbreviations: I-VII represents  $\beta$ -sheet numbers, g.l represents glycine-rich loop, c.l represents catalytic loop, GK represents gatekeeper residue, and xDFG represents highly conserved kinase residues, linker represents the loop that connects the hinge domain to  $\alpha$ C-helix. Gray dashed lines represent Van der Waals interactions. Blue lines represent hydrogen bonds and water bridges. Yellow dashed lines represent salt bridges. The cyan line represents orthogonal multipolar interaction. MD-derived occupancy values are shown on each interaction. Block III: RMSD plots of the compounds in MD simulations: (F) capivasertib and (G) *MOL\_01\_027820* in each MD simulation. The illustration of rotation by RMSF plots of compounds: (H) capivasertib and (I) *MOL\_01\_027820* for different binding patterns observed in MD simulations. For visual clarity, similar RMSF values on ligand atoms are calculated together.) as “active”.

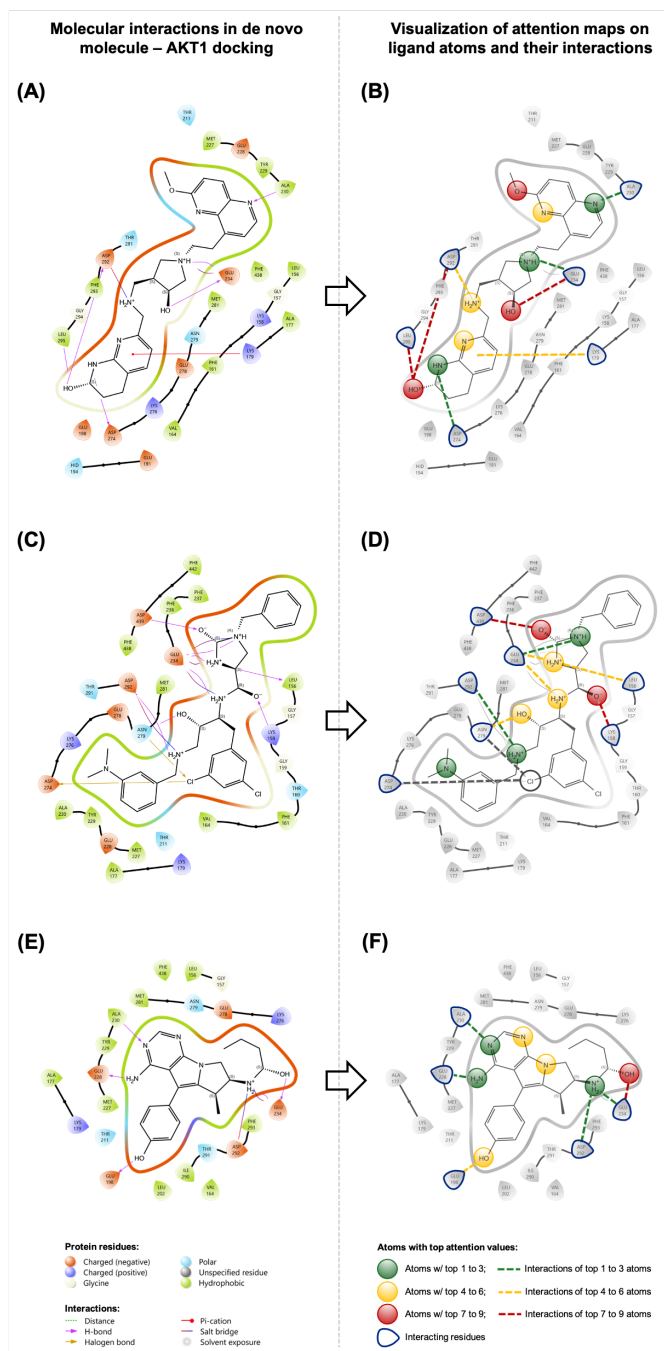


**Figure 5:** Visualisation of DrugGEN attention maps on three de novo molecules. The **left**-side column depicts protein-ligand interaction diagrams obtained from the molecular docking of DrugGEN’s three de novo molecules (in A, C and E) with the AKT1 protein structure (PDB id: “4GVI”) [42]. The docked ligands are located in the binding pocket, with interactions between residues and the ligand shown as lines, coloured by the interaction type. Protein residues are coloured according to their physicochemical properties. The **right**-side column depicts the attention maps of the same three de novo molecules (in B, D and F) retrieved from the graph transformer module of the DrugGEN generator network. Atoms that receive the highest attention scores are highlighted with colours (green: 1st, 2nd and 3rd atoms; yellow: 4th, 5th and 6th atoms; and red: 7th, 8th and 9th atoms with the highest attention scores). Atoms with lower attention scores are not coloured. In the right-side plots, receptor-ligand interactions (i.e., those obtained from the docking analysis) are represented by dashed lines in the attention-score-based colour of the molecule atom involved in the respective interaction. If an interacting atom could not be retrieved (i.e., the atom received a low attention score), its interaction is given in grey colour. **(A, B)** molecule id: *MOL\_02\_045597*, docking score: -9.803 kcal/mol, **(C, D)** molecule id: *MOL\_02\_000496*, docking score: -9.693 kcal/mol, **(E, F)** molecule id: *MOL\_02\_008350*, docking score: -9.619 kcal/mol.

### 3 Discussion and Conclusion

In this study, we developed the DrugGEN system to generate target-centric drug-like molecules automatically. DrugGEN combines the GAN architecture with graph transformers to create an end-to-end system that can design novel ligands given the target protein. DrugGEN is trained and evaluated to generate new ligands of the AKT1 protein. DrugGEN displayed a better performance compared to SOTA models in fundamental performance metrics, pointing to its high generation efficiency and capacity. Considering physicochemical metrics and structural/topological features, we showed that the DrugGEN model can generate de novo molecules with similar molecular characteristics to real inhibitors of the AKT1 protein. Further in silico analyses (i.e., molecular docking and MD simulations) were conducted to assess the interaction-related characteristics of de novo molecules, the results of which indicated their high potential in AKT1 targeting. Intending to present a tool to the community, we openly shared the code base, datasets, all results and trained models in our code repository at <https://github.com/HUBioDataLab/DrugGEN> and as a web-based tool with a graphical interface at <https://huggingface.co/spaces/HUBioDataLab/DrugGEN> where users can easily generate de novo molecules via employing the desired DrugGEN model. Our downstream analysis pipeline (Figure 1B and C) can be used to select the best drug candidate molecules from the large-scale output of any generative molecule design model in a hierarchical manner to be directed to the synthesis and wet-lab validation steps.

One essential point is that, unlike many previous generative models, DrugGEN operates at large molecular sizes similar to actual drugs and drug-like bioactive compounds (Figure S8) at the maximum size of 45 heavy atoms so that its output can be useful under different contexts even though this choice elevated the complexity of the problem. At this point, an important question is what steps should be taken after obtaining the de novo molecule records from a generative model so that they could ultimately be utilised in real-world applications of drug discovery, biotechnology or material science. In this work, we touched on this topic and proposed an in silico downstream analysis pipeline (Figure 1B and C) for an early selection of promising molecules. Our pipeline can be employed to select the best drug candidate molecules from the large-scale output of any generative model in a hierarchical manner to be directed to the synthesis and wet-lab validation steps.

Considering limitations, the adversarial training principle of GANs presented challenges, including significant divergence between the generator and discriminator losses, mode collapse, and the vanishing gradient [59, 60, 61]. However, adopting the Wasserstein GAN with gradient penalty (WGAN-GP) [62] has proven effective in mitigating these issues. This study employed random real molecular graphs as input to the generator network instead of noise. The utilisation of large molecular graphs (i.e., composed of 45 heavy atoms) elevates the complexity of the generative task, making it highly difficult for the model to find a mapping between the input noise and the high dimensional latent space of drug-like small molecules. On the other hand, learning the mapping between random small molecules and the ones that are binders of the selected target is considered a more approachable problem, which yielded high scores in the end.

In further studies, we plan to design and train: (i) DrugGEN models for other target proteins in the human proteome; (ii) GAN models that utilise sequence-based transformers using a valid and robust molecular notation such as SELFIES [63] together with a successful molecular representation learning model, e.g., SELFormer [64]; (iii) models that utilise fragments/ sub-structures of molecules as its building blocks, instead of individual atoms and bonds, to be able to generate highly synthesisable de novo compounds. Additionally, we plan to incorporate target protein features into the molecule generation process directly -also adopted in conventional structure-based drug design- to yield more successful learning regarding molecular structural constraints. Finally, we plan to improve the molecular generation process by incorporating the high-level functional properties of real drugs and drug candidate molecules (along with their structural features) into the model training procedure in the context of heterogeneous biomedical knowledge graphs [65]. This architecture is intended to facilitate understanding the relationships between the structural and functional properties of small molecules and thereby enhance the design process.

## 4 Methods

### 4.1 Datasets

Two types of data (i.e., compounds and target-based bioactivities) were retrieved from different data sources to train our deep generative models. The compound data, which includes atomic, physicochemical, and structural properties of drug and drug candidate molecules, represent our “real” samples. The compound dataset was retrieved from ChEMBL [66] (v29), an open-access chemistry database containing curated high-quality data regarding drug-like small molecules and their experimentally measured activities on biological targets. The heavy atom distribution histogram of the ChEMBL dataset is given in Figure S8, which is used to determine the threshold for the maximum number of heavy atoms in a molecule to be utilised in our model. Based on the median value and standard deviation (std) of this distribution, we selected 45 heavy atoms as our threshold (i.e., mean + 2 std) and finalised our dataset with 1,588,865 small molecules.

Experimental bioactivities, i.e., quantitative measurements of physical interactions between drug-like compounds and their target proteins, are the second data type used in the training of DrugGEN. The bioactivity data was also retrieved from the ChEMBL database. We applied various filters for standardisation, such as target type: “single protein”, assay type: “binding assay”, standard type: “=”, and pChEMBL value: “not null” (i.e., roughly correspond to curated activity data points). Then, bioactivity data belonging to the AKT1 target protein were selected from the filtered bioactivity dataset. The finalised dataset contains ligand interactions of the human AKT1 (“CHEMBL4282”) protein with a pChEMBL value equal to or greater than 6 (i.e.,  $IC_{50} \leq 1 \mu M$ ) as well as SMILES notations of these ligands. This activity dataset was extended by adding the drug molecules sourced from the DrugBank database [67] that are known to interact with human AKT1 protein. The filtering process excluded molecules larger than 45 heavy atoms and resulted in a dataset of 2,405 active/interacting small molecule ligands to train generative models tailored to AKT. Their heavy atom size distribution is given in Figure S8.

### 4.2 Graph Encodings (Featurization)

In DrugGEN, input molecules are represented as graphs, each composed of two parts: an annotation matrix (which contains information about the atom features) and an adjacency matrix (which includes information on the presence of atomic bonds and their features). The annotation and adjacency matrices of the compounds were generated using the RDKit [68] 67 library and the SMILES representation of molecules. The annotation matrix has a size of 45 by 9, representing the maximum length (the number of heavy atoms) of the molecule and nine types of atoms (i.e., C, O, N, F, S, P, Cl, I, and the null / no atoms case), respectively. These one-hot-encoded atom types are used as node features of the molecule graphs. The adjacency matrix is 45 by 45 by 5, displaying the bond information of the respective atoms of the molecule (cells of the one hot encoded third dimension of the tensor; 0th: no bond between the corresponding atoms, 1st: single, 2nd: double, 3rd: triple, and 4th: aromatic bond).

### 4.3 The Architecture of DrugGEN

The DrugGEN model is built on Generative Adversarial Networks (GAN) [9]. Figure 1D shows the overall workflow of the default DrugGEN model. The generator  $G$ , a graph transformer encoder, transforms given input  $z$  to new annotation and adjacency matrices. These matrices are then fed to the discriminator network  $D$  together with the matrices of real small molecules to assign them to the “real” and “fake” groups. The details of each module are provided below.

**Generator:** The generator ( $G$ ) module (Figure 1D) employs transformer encoder blocks [40] which operate on graph-based data [69]. For this, both the annotation and adjacency matrices are required to be processed in the same module (details regarding the dimensions and the context of annotation and adjacency matrices are given above, in the section entitled “Graph Encodings - Featurization”).  $G$  takes randomly selected real drug-like molecules from the training dataset as input instead of random noise which is usually employed as the input of the generator modules of GANs. This approach helps the model effectively handle the high complexity and sparsity of molecular graphs

(i.e.,  $45*9 + 45*45*5 = 18,630$  elements to represent a molecule). The input is fed through individual multi-layered perceptrons (MLPs) for annotation and adjacency matrices, both of which consists of four layers (i.e., input: 16, hidden1: 64, hidden2: 64, and output: 128 dimensions). These MLPs are utilized to create embeddings of annotation and adjacency matrices with  $d_k$  (default: 128) dimensions. Afterward, the input is fed to the transformer encoder module. Here, firstly, input is sent to the self attention mechanism. In the classic transformer architecture,  $Q$ ,  $K$  and  $V$  variables are the representations of the same input sequence. Attention is calculated by the scaled dot product of  $Q$  and  $K$ , after that, the attention is multiplied by  $V$  to form the final product [40]. In the graph transformer setting,  $Q_m$ ,  $K_m$  and  $V_m$  are the variables representing the annotation matrix of the molecule. However, here, attention weights are calculated as the multiplication of the adjacency matrix ( $A_m$ ) of the molecules with the scaled dot product of  $Q_m$  and  $K_m$ . Then, attention weights are multiplied with  $V_m$  to create the final representation of the annotation matrix. The new representation of the adjacency matrix is the concatenated version of the attention weights as described in the study by Dwiwedi et al. (2020) and Vignac et al. (2022) [69, 70]. For our model, output dimension size of the transformer is 128 for both the annotation and adjacency. The calculation of the attention is formulated below:

$$Attention(Q_m, K_m, V_m) = softmax\left(\frac{Q_m K_m^T}{\sqrt{d_k}} A_m\right) V_m \quad (1)$$

Where  $Q_m$ ,  $K_m$ , and  $V_m$  denote the annotation matrix of the molecules while  $A_m$  denotes their adjacency matrix.  $d_k$  is the dimension of the transformer encoder module and it is used to scale the attention weights. The reason behind multiplying the attention with the adjacency matrix via element wise multiplication is to improve the attention scores by injecting bond information into it. The attention matrix aims to identify how much each atom attends to other atoms in a pairwise manner and this is based on both short range (direct) and long range (indirect) relationships/interactions between the atoms in the molecule. Therefore, attention values can be enhanced by introducing readily available bond information between the corresponding atoms (i.e., whether an atomic bond exists or not, and if so, what specific kind of bond). This idea was first proposed in Dwivedi and Bresson (2020) [69]. After the attention layer, the final annotation and adjacency matrices undergo a process of addition and normalization. This transformation involves two main steps. First, they are passed through layer normalization, which ensures that the values within each matrix are scaled and centered appropriately. Layer normalization is formulated as follows:

$$\hat{X}^{l+1} = LayerNorm(X^l + \bar{X}^{l+1}), \hat{A}^{l+1} = LayerNorm(A^l + \bar{A}^{l+1}) \quad (2)$$

$X$  and  $A$  correspond to annotation and adjacency matrices, respectively,  $LayerNorm$  represents the layer normalisation, and  $l$  is the layer number.  $\hat{X}^{l+1}$  represents the intermediate product after the layer normalisation.  $X^l$  is the annotation matrix before attention and  $\bar{X}^{l+1}$  is the product of the attention mechanism. The same annotations are used for  $A$  (adjacency matrix).

Following this, the matrices are further processed via a feed-forward network (FFN). The FFN introduces non-linearity and learns complex representations from the input matrices, allowing higher-level feature extraction. The output of this network is then added back to the previously normalized matrices, creating a residual connection. Final matrices are passed through layer normalization at the end. The second operation can be expressed as:

$$X^{l+1} = LayerNorm(\hat{X}^{l+1} + FFN(\hat{X}^{l+1})), A^{l+1} = LayerNorm(\hat{A}^{l+1} + FFN(\hat{A}^{l+1})) \quad (3)$$

**Discriminator:** The purpose of the discriminator (D) in GANs is to compare the synthetic (fake) data,  $G(z)$ , generated by the generator with the real molecule data,  $x$ , and classify its input samples as either fake or real. The discriminator of DrugGEN (Figure 1D) is constructed using graph transformer encoder blocks, which function similarly to those of the generator. It starts by processing the annotation and adjacency matrices through linear layers in the node and edge layers to obtain the embeddings. These embeddings are then fed into the transformer encoder blocks (as described in the generator section) to transform the representations further. The discriminator is configured with a single transformer layer, featuring 8 attention heads and a hidden dimension of 128. Finally, the

output node representations are processed in a prediction head composed of an MLP (input: 64, hidden layer 1: 32, hidden layer 2: 16, and output: 1) to produce the discriminator output (i.e., prediction scores utilised for real/fake evaluation).

#### 4.4 MLP Baseline Models

The baseline model created for comparison against DrugGEN in the ablation study is a GAN with an MLP-based generator and discriminator. The architectural difference between DrugGEN and the MLP baseline is the simplified generator module. This MLP-based generator module is a modified version of the generator featured in the MolGAN study [10] and consists of two dense layers coupled with ReLU activation function ending with a dropout layer. The modification involves directly processing the starting molecules instead of employing linear projections on the noise data, as was done in MolGAN. As a result, the first dense layer, where the noise was initially processed to align its dimensions with those of flattened adjacency and annotation matrices, has been omitted. Apart from that, there is a readout layer (formed by a single dense layer) to adjust the dimension size. The MLP generator is structured with two parallel linear layers designed to handle input molecules’ annotation and adjacency matrices independently:

$$X = \text{ReadOut}(\text{DropOut}(\text{ReLU}(\text{DenseLayer}(\text{ReLU}(\text{DenseLayer}(X)))))) \quad (4)$$

$$A = \text{ReadOut}(\text{DropOut}(\text{ReLU}(\text{DenseLayer}(\text{ReLU}(\text{DenseLayer}(A)))))) \quad (5)$$

Where X and A represent annotation and adjacency matrices, respectively. Subsequently, the processed molecules follow a similar pipeline to that of the DrugGEN system, where they are passed to the discriminator for “real/fake” evaluation.

The MLP-based discriminator of the baseline model takes its input as one-dimensional vectors. Vectors representing the annotation and adjacency matrices are first flattened and then concatenated. The MLP discriminator is configured with hidden layers composed of 256, 128, 64, 32, and 16 neurons, followed by an output layer with a single neuron. This is followed by the tanh activation function to map each sample to a value between [-1,1].

We trained two baseline models called MLP baseline and MLP-NoTarget baseline, analogous to DrugGEN and DrugGEN-NoTarget, respectively. The implementation and training of the MLP baseline and MLP-NoTarget baseline adhere to the protocols used for DrugGEN, including the datasets, to ensure a fair comparison. The results obtained from baseline models are discussed in the ablation study.

#### 4.5 Loss Function

Both DrugGEN and the baseline models utilize the WGAN loss in model training [62]. The formulation of the WGAN loss for the end-to-end training of DrugGEN, is given below:

$$L = (\mathbb{E}_{x \sim p_r(x)}[D_1(x)] - \mathbb{E}_{z \sim p_g(z)}[D_1(G_1(z))]) \quad (6)$$

where  $x$  denotes real molecules, which are experimentally validated inhibitors of the target of interest, that has been used in the discriminator of DrugGEN;  $z$  denotes the input distribution of the generator;  $p_r$  denotes real data distribution and  $p_g$  the generated data distribution. It has been shown in the literature that using gradient penalty (GP) improves the performance of WGAN [71]. Due to this, we utilized GP, and its loss is formulated as:

$$L_{GP} = \lambda \mathbb{E}_{\hat{x} \sim p_{\hat{x}}(\hat{x})} [(\|\nabla_{\hat{x}} \tilde{D}(\hat{x})\|_2 - 1)^2] \quad (7)$$

where  $\lambda$  denotes a penalty coefficient;  $\hat{x}$  denotes data coming from: (i)  $x$  (real data), and (ii) generated samples.  $p_{\hat{x}}(\hat{x})$  refers to sampling uniformly along straight lines between pairs of points from the

data distribution  $p_r$  and generator distribution  $p_g$  [71]. We obtained our finalised loss function as via combining the losses given in Eqn. 6 and Eqn. 7:

$$L_{total} = L + L_{GP} \quad (8)$$

#### 4.6 The Training Scheme and Hyperparameters

DrugGEN was trained with the ChEMBL compounds dataset (used as the real molecule input of the model). The ChEMBL dataset was divided randomly into training and test partitions, maintaining a ratio of 90% and 10%, respectively. DrugGEN commences the training with  $D$  (using randomly sampled molecules from the untrained generator and real samples), and subsequently progresses to  $G$ . The AdamW optimizer [72] was employed with default parameters and a batch size of 128 was used. The entire training spanned 100 epochs; however, we utilised early stopping based on the validity and novelty metrics. This was mainly applied to prevent mode collapse. During the hyperparameter optimisation phase, various learning rates (1e-05, 5e-06, 1e-07, 0.0005, 0.0001, 0.005, and 0.001) were independently tested for each module. Finally, a learning rate of 1e-05 was chosen for all modules (both for G and D), mainly due to yielding module stability. The impact of different attention head numbers (4, 8, and 16) was explored to gauge their effect on model performance, and findings supported using 8 attention heads consistently across all models. Various embedding dimension sizes (16, 32, 64, 128, and 256) were evaluated for their impact on model behaviour. The analysis indicated that the embedding dimension size of 128 were optimal for both DrugGEN and DrugGEN-NoTarget models. Model depth was subject to experimentation with full model training, exploring the values of 1, 2, 4, and 8 to understand their influence on performance (results can be found at Table S1). We observed that higher depth values impeded the model’s convergence. As a result, a transformer depth of 1 was selected for the primary model. Training the reported DrugGEN and DrugGEN-NoTarget models required approximately 2-3 days each, using a single NVIDIA A5000 GPU (24 Gb VRAM). All analyses mentioned above were conducted as short/quick tests due to long training durations on our infrastructure. During inference, de novo molecules underwent correction to eliminate SMILES-based errors, facilitated by the UnCorrupt SMILES model [73]. Due to the requirement of the molecular analysis libraries we utilised, such as RDKit [68], back and forth conversion between graphs and SMILES was necessary at various stages of model training and validation.

#### 4.7 Performance Metrics

The performance of the models was evaluated using two sets of metrics. The first set includes four fundamental molecular generation metrics presented from the MOSES benchmark platform [43], validity, uniqueness, internal diversity (IntDiv), and novelty. These metrics are used to assess the efficiency of the generative capabilities of models and are generally concerned with the structural properties of de novo generated molecules. Validity is calculated as the percent of the data that the RDKit’s SMILES conversion function can successfully parse [68]. Uniqueness is the metric that checks whether there are redundant molecules in the same generated batch (i.e., molecules that are identical to each other), whereas IntDiv is the measurement of the mean pairwise dissimilarity (based on Tanimoto coefficient calculated using ECFP [74] based molecular fingerprints) between each molecule pair in a particular generated batch. Novelty is the ratio of the generated molecules not presented in the real molecules dataset (used in training) to all generated molecules. This study also introduced a second novelty-related metric, "novelty against the inference set (NI)," in the ablation study. NI measures the ratio of the generated molecules that are not present among the starting molecules (i.e., real molecules used as input to the generator module during an inference run). Higher values of validity, uniqueness, IntDiv, novelty, and NI indicate better performance.

The second set of metrics concerns the physicochemical properties of de novo molecules: quantitative estimate of drug-likeness (QED) and synthetic accessibility (SA). QED computes the drug-like quality of a molecule using molecular descriptors such as molecular weight, lipophilicity, hydrogen bond donors and acceptors, polar surface area (PSA), and others. The SA score assesses the difficulty of synthesising de novo generated molecules by comparing them with labelled molecular building blocks.

Higher values of QED and lower values of SA indicate better performance. Detailed descriptions of the metrics can be found in Polykovskiy et al. [43] and Landrum [68].

#### 4.8 Molecule Docking

For the docking study, the crystal structure of the selected target protein, AKT1 (PDB code “4GV1”) [42], was prepared by Protein Preparation Wizard Madhavi [75] in the Schrödinger Suite 2022-4 [76] with the OPLS4 force field. Missing hydrogen atoms were added, and water molecules were removed. The physical condition of pH was set as  $7.4 \pm 1.0$  for atom typing. The binding site of AKT1 was defined as Ala177, Lys179, Lys182, Ala212, Glu228, Ala230, Glu234, Glu278, Thr291, Asp292, by cross checking with the binding data published in the literature [42]. These findings were utilized for grid generation. Glide software [77] was used to find the best binding poses for each ligand. Van der Waals radius scaling factor was set to 1.0 and partial charge cut-off value was set to 0.25. The docking calculations were made in the Standard Precision Mode (GlideScore SP). Results were visualized via PyMOL [78].

#### 4.9 Bioactivity Prediction Procedure

Both real and de novo molecules were subjected to deep learning-based drug-target interaction (DTI) prediction against the selected protein (AKT1). We employed our previously developed DTI prediction system entitled DEEPScreen for this purpose. Briefly, DEEPScreen employs 2-D image-based structural Kakule representations (300-by-300 pixels) of compounds (created by RDKit, Draw.MolToFile function) as input and processes them via deep convolutional neural networks to classify them as active or inactive against the target of interest [56]. For this, we first trained a DEEPScreen model for the AKT1 protein using experimental bioactivity data available in ChEMBL (v30). The training data comprised 1338 active and 1666 inactive small molecules (activity threshold was selected as pChEMBL value: 7, equivalent to 100 nM concentration in terms of IC<sub>50</sub>). The high pChEMBL threshold was chosen to maximise the activity prediction confidence. We randomly split the compound dataset into train, validation and test folds (80%, 10% and 10% of the data, respectively). We augmented the dataset by adding transformed versions of each active and inactive molecule created by 10-degree rotations (the images were rotated around the centre of the image), making a total of 36 images for each input sample. This was done to render the model rotation invariant. Other types of image transformations, such as translation, were irrelevant to our case since the 2-D image generation function of RDKit standardises the molecular drawings. We optimised hyper-parameters of the model with respect to the classification metrics on the validation fold and measured the finalised performance of the model on the independent hold-out test fold. The test performance of the model was found to be precision: 0.91, recall: 0.92, F1-score: 0.92, and MCC: 0.85, which was considered highly satisfactory. Afterwards, the 2-D structural images of the real and de novo molecules were generated using the same parameters of RDKit Draw.MolToFile. The images were run on the trained AKT1 model in the prediction mode. Details regarding the DEEPScreen system and its training can be obtained from Rifaioğlu et al. [56].

#### 4.10 Molecular Dynamics Simulations

To conduct molecular dynamics (MD) simulations, firstly, AKT1 bound complexes of both compounds (capiasertib and *MOL\_01\_027820*) were aligned. Later, the simulation system was prepared with the builtin System Builder utility of Desmond 7.3. Water molecules were placed, and Na<sup>+</sup> ions were added to neutralize the system. A five step simulation relaxation protocol was applied based on the generated complex: (i) Brownian Dynamics was utilized at 10 K with NVT ensemble and Berendsen thermostat with small timesteps and restraints were applied on solute heavy atoms with 50.0 kcal/(mol Å<sup>2</sup>) force constant for 1 ns; (ii) the relaxation proceeded with Langevin dynamics with the NVT ensemble and Berendsen thermostat at 10 K for 120 ps, harmonic restraints continued to be applied; (iii) Langevin dynamics proceeded with NPT ensemble using Berendsen thermostat and barostat at 10 K for 120 ps with solvent restraints; (iv) the simulation started to be annealed with NPT ensemble using Berendsen thermostat and barostat for 120 ps by keeping the restraints; and (v) the solute heavy atoms were unrestrained and heating proceeded and reached to 300K with NPT ensemble using Nosé–Hoover thermostat, and Martyna–Tobias–Klein barostat for 240 ps with Langevin dynamics. Following the relaxation steps, 500ns MD simulations were run with NPT ensemble at 300K with Desmond 7.3. In total, four copies of the simulations were run for each

system. The trajectory visualization was done with Maestro 13.5 [76]. The simulation analyses were done with the Simulation Interactions Diagram module integrated in Maestro 13.5 [79]. Desmond Trajectory Clustering utility was applied to obtain the highest occurring conformers of the ligands during each simulation.

## 5 Data availability

The data and code to reproduce the experiments are available at the DrugGEN GitHub repo <https://github.com/HUBioDataLab/DrugGEN>, together with the results obtained. We used open-access data for input as described in Methods.

## 6 Code availability

The source code and ready-to-use trained models are available at the DrugGEN GitHub repo: <https://github.com/HUBioDataLab/DrugGEN>. DrugGEN is also available as an online tool with a graphical interface at <https://huggingface.co/spaces/HUBioDataLab/DrugGEN>, where users can generate de novo molecules by employing the desired DrugGEN model.

## 7 Acknowledgments

This project was supported by TUBITAK-BIDEB 2247-A National Leader Researchers Program under project number 120C123.

## 8 Author Information & Contributions

AU: Atabey Ünlü (atabeyunlu36@gmail.com),  
EC: Elif Çevrim (candaselif@gmail.com),  
AS: Ahmet Sarıgün (ahmet.sarigun@metu.edu.tr),  
MGY: Melih Gokay Yigit (gokay.yigit@metu.edu.tr),  
HC: Hayriye Çelikkilek (hayriye.celikkilek@gmail.com),  
OB: Osman Bayram (osmanfbayram@gmail.com),  
HAG: Heval Ataş Güvenilir (hevalatas@gmail.com),  
AK: Altay Koyaş (altay.koyas@metu.edu.tr),  
DCK: Deniz Cansen Kahraman (cansen@metu.edu.tr),  
AO: Abdurrahman Olğaç (aolgac@gazi.edu.tr),  
ASR: Ahmet Rifaioğlu (ahmet.rifaioğlu@uni-heidelberg.de),  
EB: Erden Banoğlu (banoglu@gazi.edu.tr)  
TD: Tunca Doğan (tuncadogan@gmail.com).

TD conceptualised the study and designed the general methodology. EC and HAG prepared the datasets and handled the protein featurisation process. AS, AU, ASR and TD determined the technical details of the fundamental model architecture. AU and AS prepared the original codebase and designed and implemented initial models. AU and MGY designed, implemented, trained, tuned and evaluated numerous model variants and constructed the finalised DrugGEN models. DCK and AK selected the protein target by reviewing the literature. AO and EC conducted the molecular filtering operations and physics-based (docking and molecular dynamics) experiments. HC and AU analysed the de novo generated molecules in the context of deep learning-based drug-target interaction prediction. AU, EC, AO, EB and TD evaluated and discussed the findings. EC, AU, AS and TD visualised the results and prepared the figures in the manuscript. AU, EC, AS, HC, HAG, AO and TD wrote the manuscript. AU, EC, AS, MGY and TD prepared the repository. OB and MGY constructed the online tool. TD, AO, EB and ASR supervised the overall study. All authors approved the manuscript.

## References

- [1] Ahmet Sureyya Rifaioglu, Heval Atas, Maria Jesus Martin, Rengul Cetin-Atalay, Volkan Atalay, and Tunca Doğan. Recent applications of deep learning and machine intelligence on in silico drug discovery: methods, tools and databases. *Briefings in Bioinformatics*, 20(5):1878–1912, September 2019.
- [2] Steven M. Paul, Daniel S. Mytelka, Christopher T. Dunwiddie, Charles C. Persinger, Bernard H. Munos, Stacy R. Lindborg, and Aaron L. Schacht. How to improve r&d productivity: the pharmaceutical industry’s grand challenge. *Nature reviews Drug discovery*, 9(3):203–214, 2010.
- [3] Govinda Bhisetti and Cheng Fang. Artificial intelligence-enabled de novo design of novel compounds that are synthesizable. *Artificial Intelligence in Drug Design*, page 409–419, 2022.
- [4] Daniel C. Elton, Zois Boukouvalas, Mark D. Fuge, and Peter W. Chung. Deep learning for molecular design—a review of the state of the art. *Molecular Systems Design & Engineering*, 4(4):828–849, 2019.
- [5] W. Patrick Walters. Virtual chemical libraries: miniperspective. *Journal of medicinal chemistry*, 62(3):1116–1124, 2018.
- [6] Varnavas D. Mouchlis, Antreas Afantitis, Angela Serra, Michele Fratello, Anastasios G. Papatiamantis, Vassilis Aidinis, Iseult Lynch, Dario Greco, and Georgia Melagraki. Advances in de novo drug design: from conventional to machine learning methods. *International journal of molecular sciences*, 22(4):1676, 2021.
- [7] Diederik P. Kingma and Max Welling. Auto-encoding variational bayes. *arXiv preprint arXiv:1312.6114*, 2013.
- [8] Rafael Gómez-Bombarelli, Jennifer N. Wei, David Duvenaud, José Miguel Hernández-Lobato, Benjamín Sánchez-Lengeling, Dennis Sheberla, Jorge Aguilera-Iparraguirre, Timothy D. Hirzel, Ryan P. Adams, and Alán Aspuru-Guzik. Automatic chemical design using a data-driven continuous representation of molecules. *ACS Central Science*, 4(2):268–276, February 2018.
- [9] Ian Goodfellow, Jean Pouget-Abadie, Mehdi Mirza, Bing Xu, David Warde-Farley, Sherjil Ozair, Aaron Courville, and Yoshua Bengio. Generative adversarial networks. *Communications of the ACM*, 63(11):139–144, October 2020.
- [10] Nicola De Cao and Thomas Kipf. Molgan: An implicit generative model for small molecular graphs. *arXiv preprint arXiv:1805.11973*, 2018.
- [11] Jinping Zou, Jialin Yu, Pengwei Hu, Long Zhao, and Shaoping Shi. Stagan: An approach for improve the stability of molecular graph generation based on generative adversarial networks. *Computers in Biology and Medicine*, 167:107691, 2023.
- [12] Omar Mahmood, Elman Mansimov, Richard Bonneau, and Kyunghyun Cho. Masked graph modeling for molecule generation. *Nature Communications*, 12(1):3156, May 2021.
- [13] Jonathan Ho, Ajay Jain, and Pieter Abbeel. Denoising diffusion probabilistic models. In H. Larochelle, M. Ranzato, R. Hadsell, M. F. Balcan, and H. Lin, editors, *Advances in Neural Information Processing Systems*, volume 33, page 6840–6851. Curran Associates, Inc., 2020.
- [14] Jascha Sohl-Dickstein, Eric Weiss, Niru Maheswaranathan, and Surya Ganguli. Deep unsupervised learning using nonequilibrium thermodynamics. In *Proceedings of the 32nd International Conference on Machine Learning*, page 2256–2265. PMLR, June 2015.
- [15] Emiel Hooeboom, Victor Garcia Satorras, Clément Vignac, and Max Welling. Equivariant diffusion for molecule generation in 3d. In *Proceedings of the 39th International Conference on Machine Learning*, page 8867–8887. PMLR, June 2022.
- [16] Xingang Peng, Shitong Luo, Jiaqi Guan, Qi Xie, Jian Peng, and Jianzhu Ma. Pocket2mol: Efficient molecular sampling based on 3d protein pockets. In *International Conference on Machine Learning*, pages 17644–17655. PMLR, 2022.
- [17] Arne Schneuing, Yuanqi Du, Charles Harris, Arian Jamasb, Ilia Igashov, Weitao Du, Tom Blundell, Pietro Lió, Carla Gomes, Max Welling, et al. Structure-based drug design with equivariant diffusion models. *arXiv preprint arXiv:2210.13695*, 2022.
- [18] Raghunathan Ramakrishnan, Pavlo O. Dral, Matthias Rupp, and O. Anatole Von Lilienfeld. Quantum chemistry structures and properties of 134 kilo molecules. *Scientific data*, 1(1):1–7, 2014.

- [19] Lars Ruddigkeit, Ruud Van Deursen, Lorenz C. Blum, and Jean-Louis Reymond. Enumeration of 166 billion organic small molecules in the chemical universe database gdb-17. *Journal of chemical information and modeling*, 52(11):2864–2875, 2012.
- [20] Joshua Mitton, Hans M. Senn, Klaas Wynne, and Roderick Murray-Smith. A graph vae and graph transformer approach to generating molecular graphs. *arXiv preprint arXiv:2104.04345*, 2021.
- [21] Kohei Nemoto and Hiromasa Kaneko. De novo direct inverse qspr/qsar: Chemical variational autoencoder and gaussian mixture regression models. *Journal of Chemical Information and Modeling*, 63(3):794–805, 2023.
- [22] Ryan J. Richards and Austen M. Groener. Conditional  $\beta$ -vae for de novo molecular generation. *arXiv preprint arXiv:2205.01592*, 2022.
- [23] Artur Kadurin, Sergey Nikolenko, Kuzma Khrabrov, Alex Aliper, and Alex Zhavoronkov. drugan: An advanced generative adversarial autoencoder model for de novo generation of new molecules with desired molecular properties in silico. *Molecular Pharmaceutics*, 14(9):3098–3104, September 2017.
- [24] Xuezhi Xie, Pedro A. Valiente, and Philip M. Kim. Helixgan a deep-learning methodology for conditional de novo design of  $\alpha$ -helix structures. *Bioinformatics*, 39(1):btad036, 2023.
- [25] Josep Arús-Pous, Simon Viet Johansson, Oleksii Prykhodko, Esben Jannik Bjerrum, Christian Tyrchan, Jean-Louis Reymond, Hongming Chen, and Ola Engkvist. Randomized smiles strings improve the quality of molecular generative models. *Journal of cheminformatics*, 11(1):1–13, 2019.
- [26] Viraj Bagal, Rishal Aggarwal, P. K. Vinod, and U. Deva Priyakumar. Molgpt: Molecular generation using a transformer-decoder model. *Journal of Chemical Information and Modeling*, 62(9):2064–2076, May 2022.
- [27] Thomas Blaschke, Josep Arús-Pous, Hongming Chen, Christian Margreitter, Christian Tyrchan, Ola Engkvist, Kostas Papadopoulos, and Atanas Patronov. Reinvent 2.0: an ai tool for de novo drug design. *Journal of chemical information and modeling*, 60(12):5918–5922, 2020.
- [28] Xun Wang, Changnan Gao, Peifu Han, Xue Li, Wenqi Chen, Alfonso Rodríguez Patón, Shuang Wang, and Pan Zheng. Petrans: De novo drug design with protein-specific encoding based on transfer learning. *International Journal of Molecular Sciences*, 24(2):1146, 2023.
- [29] Odin Zhang, Jintu Zhang, Jieyu Jin, Xujun Zhang, RenLing Hu, Chao Shen, Hanqun Cao, Hongyan Du, Yu Kang, Yafeng Deng, et al. Resgen is a pocket-aware 3d molecular generation model based on parallel multiscale modelling. *Nature Machine Intelligence*, 5(9):1020–1030, 2023.
- [30] Jiaqi Guan, Wesley Wei Qian, Xingang Peng, Yufeng Su, Jian Peng, and Jianzhu Ma. 3d equivariant diffusion for target-aware molecule generation and affinity prediction. (arXiv:2303.03543), March 2023. arXiv:2303.03543 [cs, q-bio].
- [31] Quentin Perron, Olivier Mirguet, Hamza Tajmouati, Adam Skiredj, Anne Rojas, Arnaud Gohier, Pierre Ducrot, Marie-Pierre Bourguignon, Patricia Sansilvestri-Morel, and Nicolas Do Huu. Deep generative models for ligand-based de novo design applied to multi-parametric optimization. *Journal of Computational Chemistry*, 43(10):692–703, 2022.
- [32] Niklas W. A. Gebauer, Michael Gastegger, Stefaan S. P. Hessmann, Klaus-Robert Müller, and Kristof T. Schütt. Inverse design of 3d molecular structures with conditional generative neural networks. *Nature Communications*, 13(1):973, February 2022.
- [33] Yueshan Li, Liting Zhang, Yifei Wang, Jun Zou, Ruicheng Yang, Xinling Luo, Chengyong Wu, Wei Yang, Chenyu Tian, and Haixing Xu. Generative deep learning enables the discovery of a potent and selective ripk1 inhibitor. *Nature Communications*, 13(1):6891, 2022.
- [34] Meng Liu, Youzhi Luo, Kanji Uchino, Koji Maruhashi, and Shuiwang Ji. Generating 3d molecules for target protein binding. (arXiv:2204.09410), May 2022. arXiv:2204.09410 [cs, q-bio].
- [35] Eyal Rozenberg and Daniel Freedman. Semi-equivariant conditional normalizing flows, with applications to target-aware molecule generation. *Machine Learning: Science and Technology*, 4(3):035037, 2023.

- [36] Wentao Shi, Manali Singha, Gopal Srivastava, Limeng Pu, J. Ramanujam, and Michal Brylinski. Pocket2drug: an encoder-decoder deep neural network for the target-based drug design. *Frontiers in pharmacology*, 13:837715, 2022.
- [37] Gökçe Uludoğan, Elif Ozkirimli, Kutlu O Ulgen, Nilgün Karalı, and Arzucan Özgür. Exploiting pretrained biochemical language models for targeted drug design. *Bioinformatics*, 38(Supplement2), 2022.
- [38] Mingyang Wang, Chang-Yu Hsieh, Jike Wang, Dong Wang, Gaoqi Weng, Chao Shen, Xiaojun Yao, Zhitong Bing, Honglin Li, Dongsheng Cao, and Tingjun Hou. Relation: A deep generative model for structure-based de novo drug design. *Journal of Medicinal Chemistry*, 65(13):9478–9492, July 2022.
- [39] Yunjiang Zhang, Shuyuan Li, Miaojuan Xing, Qing Yuan, Hong He, and Shaorui Sun. Universal approach to de novo drug design for target proteins using deep reinforcement learning. *ACS omega*, 8(6):5464–5474, 2023.
- [40] Ashish Vaswani, Noam Shazeer, Niki Parmar, Jakob Uszkoreit, Llion Jones, Aidan N. Gomez, Łukasz Kaiser, and Illia Polosukhin. Attention is all you need. *Advances in neural information processing systems*, 30, 2017.
- [41] Thomas N. Kipf and Max Welling. Semi-supervised classification with graph convolutional networks. *arXiv preprint arXiv:1609.02907*, 2016.
- [42] Matt Addie, Peter Ballard, David Buttar, Claire Crafter, Gordon Currie, Barry R. Davies, Judit Debreczeni, Hannah Dry, Philippa Dudley, Ryan Greenwood, Paul D. Johnson, Jason G. Kettle, Clare Lane, Gillian Lamont, Andrew Leach, Richard W. A. Luke, Jeff Morris, Donald Ogilvie, Ken Page, Martin Pass, Stuart Pearson, and Linette Ruston. Discovery of 4-amino- n -[(1 s )-1-(4-chlorophenyl)-3-hydroxypropyl]-1-(7 h -pyrrolo[2,3- d ]pyrimidin-4-yl)piperidine-4-carboxamide (azd5363), an orally bioavailable, potent inhibitor of akt kinases. *Journal of Medicinal Chemistry*, 56(5):2059–2073, March 2013.
- [43] Daniil Polykovskiy, Alexander Zhebrak, Benjamin Sanchez-Lengeling, Sergey Golovanov, Oktai Tatanov, Stanislav Belyaev, Rauf Kurbanov, Aleksey Artamonov, Vladimir Aladinskiy, Mark Veselov, Artur Kadurin, Simon Johansson, Hongming Chen, Sergey Nikolenko, Alán Aspuru-Guzik, and Alex Zhavoronkov. Molecular sets (moses): A benchmarking platform for molecular generation models. *Frontiers in Pharmacology*, 11:565644, December 2020.
- [44] Gabriel Lima Guimaraes, Benjamin Sanchez-Lengeling, Carlos Outeiral, Pedro Luis Cunha Farias, and Alán Aspuru-Guzik. Objective-reinforced generative adversarial networks (organ) for sequence generation models. (arXiv:1705.10843), February 2018. arXiv:1705.10843 [cs, stat].
- [45] Yi Fang, Xiaoyong Pan, and Hong-Bin Shen. De novo drug design by iterative multiobjective deep reinforcement learning with graph-based molecular quality assessment. *Bioinformatics*, 39(4):btad157, April 2023.
- [46] Zhenpeng Zhou, Steven Kearnes, Li Li, Richard N. Zare, and Patrick Riley. Optimization of molecules via deep reinforcement learning. *Scientific Reports*, 9(1):10752, July 2019.
- [47] Francesca Grisoni, Michael Moret, Robin Lingwood, and Gisbert Schneider. Bidirectional molecule generation with recurrent neural networks. *Journal of Chemical Information and Modeling*, 60(3):1175–1183, March 2020.
- [48] Yutong Xie, Chence Shi, Hao Zhou, Yuwei Yang, Weinan Zhang, Yong Yu, and Lei Li. Mars: Markov molecular sampling for multi-objective drug discovery. (arXiv:2103.10432), March 2021. arXiv:2103.10432 [cs, q-bio].
- [49] Marcus Olivecrona, Thomas Blaschke, Ola Engkvist, and Hongming Chen. Molecular de-novo design through deep reinforcement learning. *Journal of Cheminformatics*, 9(1):48, December 2017.
- [50] Leland McInnes, John Healy, and James Melville. Umap: Uniform manifold approximation and projection for dimension reduction. *arXiv preprint arXiv:1802.03426*, 2018.
- [51] Laurens Van der Maaten and Geoffrey Hinton. Visualizing data using t-sne. *Journal of machine learning research*, 9(11), 2008.

- [52] Joseph L. Durant, Burton A. Leland, Douglas R. Henry, and James G. Nourse. Reoptimization of mdl keys for use in drug discovery. *Journal of Chemical Information and Computer Sciences*, 42(6):1273–1280, November 2002.
- [53] Christopher A. Lipinski, Franco Lombardo, Beryl W. Dominy, and Paul J. Feeney. Experimental and computational approaches to estimate solubility and permeability in drug discovery and development settings. *Advanced drug delivery reviews*, 23(1–3):3–25, 1997.
- [54] Daniel F. Veber, Stephen R. Johnson, Hung-Yuan Cheng, Brian R. Smith, Keith W. Ward, and Kenneth D. Kopple. Molecular properties that influence the oral bioavailability of drug candidates. *Journal of medicinal chemistry*, 45(12):2615–2623, 2002.
- [55] Jonathan B. Baell and Georgina A. Holloway. New substructure filters for removal of pan assay interference compounds (pains) from screening libraries and for their exclusion in bioassays. *Journal of medicinal chemistry*, 53(7):2719–2740, 2010.
- [56] Ahmet Sureyya Rifaioglu, Esra Nalbat, Volkan Atalay, Maria Jesus Martin, Rengul Cetin-Atalay, and Tunca Doğan. Deepscreen: high performance drug–target interaction prediction with convolutional neural networks using 2-d structural compound representations. *Chemical science*, 11(9):2531–2557, 2020.
- [57] Vikas Sharma and Mohit Gupta. Designing of kinase hinge binders: A medicinal chemistry perspective. *Chemical Biology & Drug Design*, 100(6):968–980, 2022.
- [58] Oscar PJ Van Linden, Albert J. Kooistra, Rob Leurs, Iwan JP De Esch, and Chris De Graaf. Klifs: a knowledge-based structural database to navigate kinase–ligand interaction space. *Journal of medicinal chemistry*, 57(2):249–277, 2014.
- [59] Bhaskar Ghosh, Indira Kalyan Dutta, Michael Totaro, and Magdy Bayoumi. A survey on the progression and performance of generative adversarial networks. In *2020 11th International Conference on Computing, Communication and Networking Technologies (ICCCNT)*, page 1–8, Kharagpur, India, July 2020. IEEE.
- [60] Jie Gui, Zhenan Sun, Yonggang Wen, Dacheng Tao, and Jieping Ye. A review on generative adversarial networks: Algorithms, theory, and applications. *IEEE Transactions on Knowledge and Data Engineering*, 35(4):3313–3332, April 2023.
- [61] Giacomo Janson, Gilberto Valdes-Garcia, Lim Heo, and Michael Feig. Direct generation of protein conformational ensembles via machine learning. *Nature Communications*, 14(1):774, 2023.
- [62] Martin Arjovsky, Soumith Chintala, and Léon Bottou. Wasserstein generative adversarial networks. In *Proceedings of the 34th International Conference on Machine Learning*, page 214–223. PMLR, July 2017.
- [63] Mario Krenn, Florian Häse, AkshatKumar Nigam, Pascal Friederich, and Alan Aspuru-Guzik. Self-referencing embedded strings (selfies): A 100string representation. *Machine Learning: Science and Technology*, 1(4):045024, December 2020.
- [64] Atakan Yüksel, Erva Ulusoy, Atabey Ünlü, and Tunca Doğan. Selfformer: Molecular representation learning via selfies language models. *Machine Learning: Science and Technology*, 2023.
- [65] Tunca Doğan, Heval Atas, Vishal Joshi, Ahmet Atakan, Ahmet Sureyya Rifaioglu, Esra Nalbat, Andrew Nightingale, Rabie Saidi, Vladimir Volynkin, and Hermann Zellner. Crossbar: comprehensive resource of biomedical relations with knowledge graph representations. *Nucleic acids research*, 49(16):e96–e96, 2021.
- [66] David Mendez, Anna Gaulton, A. Patrícia Bento, Jon Chambers, Marleen De Veij, Eloy Félix, María Paula Magariños, Juan F. Mosquera, Prudence Mutowo, and Michał Nowotka. ChEMBL: towards direct deposition of bioassay data. *Nucleic acids research*, 47(D1):D930–D940, 2019.
- [67] David S Wishart, Yannick D Feunang, An C Guo, Elvis J Lo, Ana Marcu, Jason R Grant, Tanvir Sajed, Daniel Johnson, Carin Li, Zinat Sayeeda, Nazanin Assempour, Ithayavani Iynkkaran, Yifeng Liu, Adam Maciejewski, Nicola Gale, Alex Wilson, Lucy Chin, Ryan Cummings, Diana Le, Allison Pon, Craig Knox, and Michael Wilson. Drugbank 5.0: a major update to the drugbank database for 2018. *Nucleic Acids Research*, 46(D1):D1074–D1082, January 2018.
- [68] Greg Landrum. Rdkit documentation. *Release*, 1(1–79):4, 2013.

- [69] Vijay Prakash Dwivedi and Xavier Bresson. A generalization of transformer networks to graphs. (arXiv:2012.09699), January 2021. arXiv:2012.09699 [cs].
- [70] Clement Vignac, Igor Krawczuk, Antoine Siraudin, Bohan Wang, Volkan Cevher, and Pascal Frossard. Digress: Discrete denoising diffusion for graph generation. *arXiv preprint arXiv:2209.14734*, 2022.
- [71] Ishaan Gulrajani, Faruk Ahmed, Martin Arjovsky, Vincent Dumoulin, and Aaron C Courville. Improved training of wasserstein gans. In *Advances in Neural Information Processing Systems*, volume 30. Curran Associates, Inc., 2017.
- [72] Ilya Loshchilov and Frank Hutter. Decoupled weight decay regularization. *arXiv preprint arXiv:1711.05101*, 2017.
- [73] Linde Schoenmaker, Olivier JM Béquignon, Willem Jespers, and Gerard JP van Westen. Uncorrupt smiles: a novel approach to de novo design. *Journal of Cheminformatics*, 15(1):22, 2023.
- [74] David Rogers and Mathew Hahn. Extended-connectivity fingerprints. *Journal of chemical information and modeling*, 50(5):742–754, 2010.
- [75] G. Madhavi Sastry, Matvey Adzhigirey, Tyler Day, Ramakrishna Annabhimoju, and Woody Sherman. Protein and ligand preparation: parameters, protocols, and influence on virtual screening enrichments. *Journal of computer-aided molecular design*, 27:221–234, 2013.
- [76] Schrödinger Release. *1: Maestro, Schrödinger, LLC, New York, NY. 2021.* [(accessed on 10 December 2021)]. 2022.
- [77] Richard A. Friesner, Robert B. Murphy, Matthew P. Repasky, Leah L. Frye, Jeremy R. Greenwood, Thomas A. Halgren, Paul C. Sanschagrin, and Daniel T. Mainz. Extra precision glide: Docking and scoring incorporating a model of hydrophobic enclosure for protein-ligand complexes. *Journal of Medicinal Chemistry*, 49(21):6177–6196, October 2006.
- [78] L. L. C. Schrodinger. The pymol molecular graphics system. *Version*, 1:8, 2015.
- [79] Schrödinger Release. *1: Desmond Molecular Dynamics System, DE Shaw Research, New York, NY, 2021. Maestro-Desmond Interoperability Tools, Schrödinger.* 2023.

---

## SUPPLEMENTARY MATERIAL

---

### Supplementary Text

#### S1. A short review of the fundamental literature on AI-based molecule design

One of the first generative modelling architectures used in de novo molecule design was variational autoencoders (VAE) [?]. Gomez-Bombarelli et al. devised a molecule generation method based on VAE, where the encoding network converts discrete SMILES expressions of molecules into continuous vectors, with the decoder network subsequently reconstructing SMILES from this continuous space. Furthermore, an additional network was implemented to the system that guides the decoder by predicting properties such as drug-likeness and synthetic accessibility of the representations in the latent space [?]. Another generative modelling architecture, Generative Adversarial Networks (GAN) [?], originally developed for image generation, has been employed to design de novo molecules. GANs are trained via a battle between generator and discriminator networks in a zero-sum game, where each agent tries to beat the other one by performing better at each move. The model called MolGAN uses a multilayer perceptron-based generator and graph convolutional discriminator to handle the molecule generation process [?]. This method was one of the first studies to implement GANs for de novo drug design. A few GAN-based models, similar to MolGAN, were implemented in the following years [?]. Another study set the training objective as predicting the masked node and edge labels on molecular graphs to enhance the efficiency of the molecular design process [?]. Denoising diffusion probabilistic models have surfaced as a promising approach as a part of the recent advancements in generative modelling [?, ?]. Diffusion models learn the underlying data distribution by constructing a forward diffusion process and utilising a denoising model. One notable study by Hoogeboom et al. [?] proposes an equivariant diffusion model (EDM) for molecule generation in 3-D. The model uses forward diffusion to add noise to input atom coordinates and types and reverse diffusion to denoise the positions and types. This approach enables the generation of diverse molecular structures in the learned Euclidean space. Although diffusion models have the potential to provide high-quality samples, training and inference with them can be challenging due to difficulties in convergence, lengthy iterations, and the resource-intensive nature of computations. While other 3-D graph-based models exist [?, ?], their tendency to grapple with higher computational requirements and lower success rates in solving complex problems underscores the favorability of 2-D graph-based models for providing reliable approximations. This causes an overall preference for 2-D graph-based models over their 3-D counterparts, due to their ability to offer cost-effective modelling with high generalisation capabilities, facilitating rapid analysis of extensive datasets.

#### S2. About protein kinase B (PKB) / AKT

One of the intriguing proteins with biomedical relevance to be targeted in this context can be the AKT protein, also known as protein kinase B (PKB). AKT is an evolutionarily conserved serine-threonine kinase that plays a critical role in the development and progression of cancer [?]. AKT is a key component of the PI3K/AKT signalling pathway, which regulates various cellular processes such as proliferation, cell growth, metabolism, and survival [?]. The three isoforms—AKT1, AKT2, and AKT3—have distinct functions and tissue expressions, sharing a structurally conserved composition (85-90% sequence similarity) [?]. The shared compositions comprise an N-terminus PH domain, a central kinase domain, and a C-terminus regulatory domain encompassing a hydrophobic motif [?]. In numerous cancer types, the activation of AKT signalling is frequently observed, leading to

increased cell survival and uncontrolled proliferation [?, ?, ?, ?, ?]. Therefore, inhibition of AKT signalling has emerged as a promising therapeutic approach for various cancers, as targeting this pathway could inhibit tumour growth and improve the efficacy of other treatments. AKT1 inhibitors may compete with adenosine triphosphate (ATP) for its binding site in the kinase domain (Figure S1). Alternatively, they may go for allosteric binding sites (i.e., the pleckstrin homology - PH domain) [?] (Figure S1). Some important ATP-competent AKT inhibitors that reached clinical trials include uprosertib (GSK2141795), ipatasertib (GDC-0068), and capivasertib (AZD5363) 15. Recently, the latter was approved by the FDA [?]. Capivasertib and ipatasertib were also crystallised within the ATP binding site of the AKT1 protein (PDB ids: “4GV1” [?] and “4EKL” [?], respectively). Numerous studies in industry and academia highlight the current need for novel inhibitors that effectively target the AKT pathway.

### S3. Analysis of physicochemical distributions

In Figure S2, each panel displays a different physicochemical property. In the left side plot of each panel, non-targeted molecules are compared (i.e., all ChEMBL molecules in our training dataset vs. non-targeted de novo molecules generated by DrugGEN-NoTarget). In contrast, on the right side plot of each panel, targeted molecules are compared (i.e., real AKT1 inhibitors vs. targeted de novo molecules generated by DrugGEN where the starting molecules are real AKT1 inhibitors). It is observed from Figure S2 that, in general, property distributions of non-targeted de novo molecules (i.e., DrugGEN-NoTarget) are similar to ChEMBL molecules, which represent this model’s training dataset, and distributions of targeted de novo molecules (i.e., DrugGEN) resemble real AKT1 inhibitors. The real AKT1 inhibitors exhibit higher molecular weights and a greater number of heavy atoms and aromatic rings than ChEMBL molecules (e.g., Figure S2A, B and H). The same pattern is also evident in DrugGEN molecules when compared with DrugGEN-Notarget. Also, the DrugGEN model successfully learned the hydrogen bond acceptor (HBA) and hydrogen bond donor (HBD) value distributions of AKT1 inhibitors, as demonstrated in Figure S2E and F. Nevertheless, the same is not true for DrugGEN-NoTarget. Apart from that, Figure S2C displays that ChEMBL and AKT1 molecules exhibit almost identical AlogP values (i.e., a measure of the relative solubility of a molecule in two liquids: octanol and water); however, DrugGEN and DrugGEN-Notarget models both yielded a shifted mean compared to the distributions of their training datasets. Furthermore, polar surface area (PSA) (Figure S2D) and rotatable bond (RB) (Figure S2G) value distributions of DrugGEN and DrugGEN-Notarget do not reflect the ratio between AKT1 and ChEMBL datasets; therefore, we conducted a statistical analysis to observe whether there is a notable difference between DrugGEN and DrugGEN-Notarget, although the distributions of their training datasets could not be captured. According to Mann-Whitney U rank test, PSA distributions (Figure S2D) of DrugGEN and DrugGEN-Notarget are significantly different from each other (p-value < 0.0001); however, the same outcome was not obtained for RB distributions (Figure S2G) (p-value > 0.05).

### S4. Ablation study (additional comments)

As shown by the QED, and SA values in Table 2, our models display variations in physicochemical property-related metrics. QED values of DrugGEN vary between the ChEMBL dataset and the AKT1 dataset, which was to be expected given that the model uses both of these datasets during learning. Higher QED values can be interpreted as a positive result, indicating that the de novo-generated compounds align well with typical drug development requirements. From this perspective, both targeted models can be considered successful since they improve the QED value of the real AKT1 inhibitors dataset. The synthetic accessibility (SA) score quantifies the ease of synthesis; consequently, lower values are preferred. All models produced comparable results on this subject, with slightly higher values than the training datasets. MLP-Generator model performed marginally better at SA when compared to the default DrugGEN model.

### S5. Molecular dynamics simulations results (details)

By conducting MD simulations with capivasertib (PDB id: ‘4GV1’) 24, we aimed to observe whether the applied methodology was reliable in; (i) observing similar binding patterns with the adenine binding region, (ii) maintaining essential interactions with the hinge domain and other pockets, and (iii) conserving important conformations, such as  $\alpha$ C chain-in and DFG-in. The full versions of the

comments about Capiwasertib–AKT1 and *MOL\_01\_027820*–AKT1 MDs can be found below.

#### Capiwasertib–AKT1:

Capiwasertib remained stable during all simulations (RMSD <1, Figure 4 panels F and H). The interaction analysis of capiwasertib showed that hydrogen bonds with the hinge domain (via Glu228 -99%- and Ala230 -99%- residues) were conserved during the simulation. An additional hydrogen bond was seen with Glu278 (74%). Also, several water bridges were observed between the amine group located on the piperidine ring and Glu278 (74%), Asp292 (90%) residues, amide group and Lys158 (33%), Glu234 (11%), Asn279 (28%), Asp292 (36%) residues, and hydroxyl group and the Lys276 (19%) residue. The quaternary amine group formed a salt bridge with Glu294 (94%), and the p-Chlorobenzyl group showed cation- $\pi$  interactions with Lys179 (11%) (Figure 4C).

#### *MOL\_01\_027820*–AKT1:

*MOL\_01\_027820* showed two different binding patterns (pattern-1 and -2, shown in Figure 4 panels D and E, respectively). Those patterns were seen in two individual copies of the simulations. Pattern-1 was observed in the second and the third replica simulations and pattern-2 was observed in the first and the fourth replicas (Figure 4G). The first pattern was similar to the docking-derived starting conformation (RMSDaverage = 1.2, Figure 4 panels D, G, and I) and relatively close to the binding pattern with the compound capiwasertib. However, the second pattern showed 110.2 degrees of dihedral tilting (RMSDaverage 3.1, Figure 4 panels E, and G) following atom number 15 and above (Figure 4I) but still conserved the essential interactions with the hinge domain and remained within the binding cleft and conserved the protein's general conformation. The hydrogen interactions with Glu228 (54% and 65%, respectively given for pattern-1 and -2) and Ala230 (83% and 66%, respectively given for pattern-1 and -2) backbone atoms were formed (which did not exist in the docking-derived pose) with high occupancy values in the hinge domain. However, the remaining part of the molecule showed torsional rotations observed after the 12th and, more importantly, after the 16th atoms (Figure 4I). Therefore, slight differences in the bound clefts and the interaction networks were seen during simulations. Pattern-1 showed that the hydroxyl group connected to the fluorobenzyl moiety forms hydrogen bonds with Glu234 (44%) and water bridges with Lys158 (48%), Glu234 (20% and 63%), and Tyr437 (52%) with the same residue. The second hydroxyl group located at the center of the ligand showed hydrogen bonds with Leu156 (22%) and Glu234 (16%) and water bridges with Glu234 (16%) and Leu156 (19%) residues.  $\pi$ - $\pi$  interactions were seen with fluorophenyl and Phe237 (53%) and Phe442 (18%) residues (Figure 4D). In pattern-2, the water network around the acid hole (Glu234 and Asp292) was mostly broken and only two water bridges remained with Leu158 (37%) and Glu234 (10%). Hydrogen bonds were observed between the central hydroxyl group and Leu156 (11%), Glu234 (67%) residues and amine group in the heterocyclic ring and Asp292 (10%) residue. The rotated conformation was found to form Van der Waals interactions with the hydrophobic portions of the surrounding lysine residues and orthogonal multipolar interactions with fluorine atoms of the ligand and carbonyl group of Lys163 (Figure 4E).

## Supplementary Figures

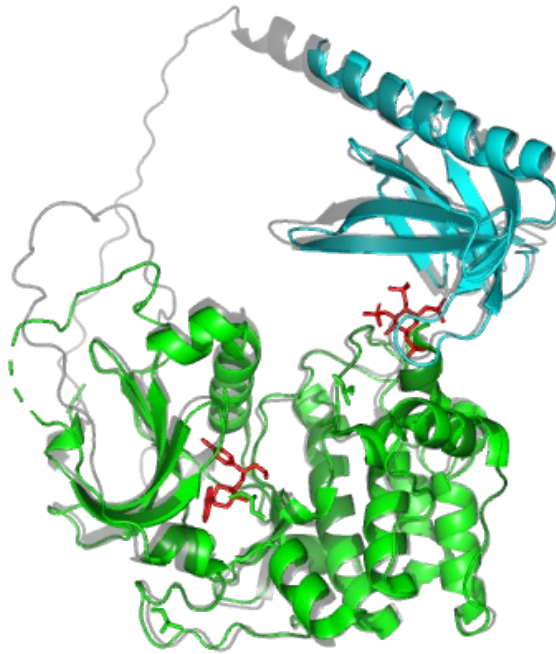


**Figure S1:** General overview of full AKT1 protein structure (gray: AlphaFold structure based on Uniprot ID: P31749, green: kinase (orthosteric) domain (PDB: 4GV1), cyan: PH (allosteric) domain (PDB: 1H10), red: ligands).

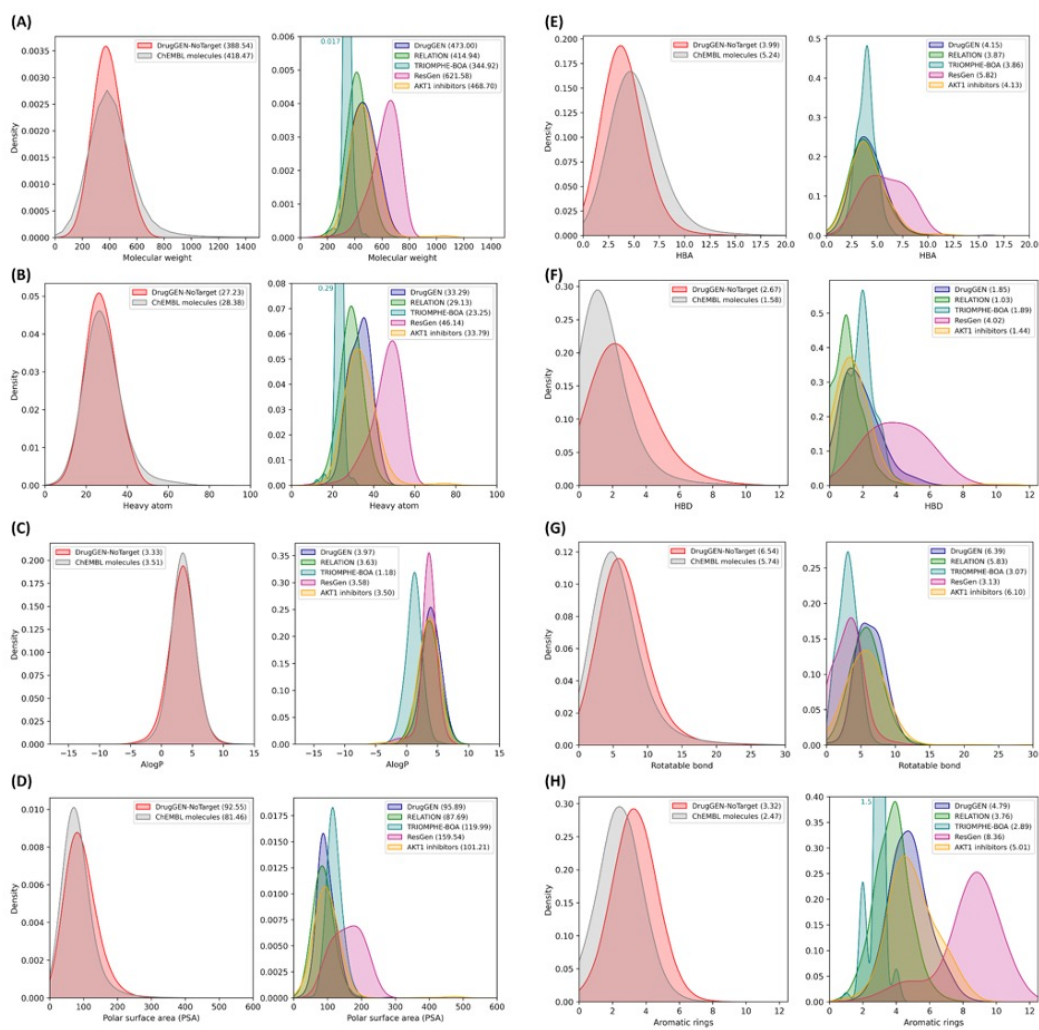


**Figure S2:** Physicochemical property value distributions of de novo molecules generated by target-centric and non-targeted models, randomly selected ChEMBL molecules and real AKT1 inhibitors for (A) molecular weight, (B) number of heavy atoms, (C) AlogP, (D) polar surface area (PSA), (E) hydrogen bond acceptor (HBA), (F) hydrogen bond donor (HBD), (G) rotatable bonds, and (H) aromatic rings. In each panel, DrugGEN-NoTarget and random ChEMBL molecules are given in the plot on the left side, whereas the targeted models' distributions are on the right side (i.e., DrugGEN, RELATION, TRIOMPHE-BOA, ResGen and real AKT1 inhibitors). The numbers in parentheses in figure legends indicate mean values.

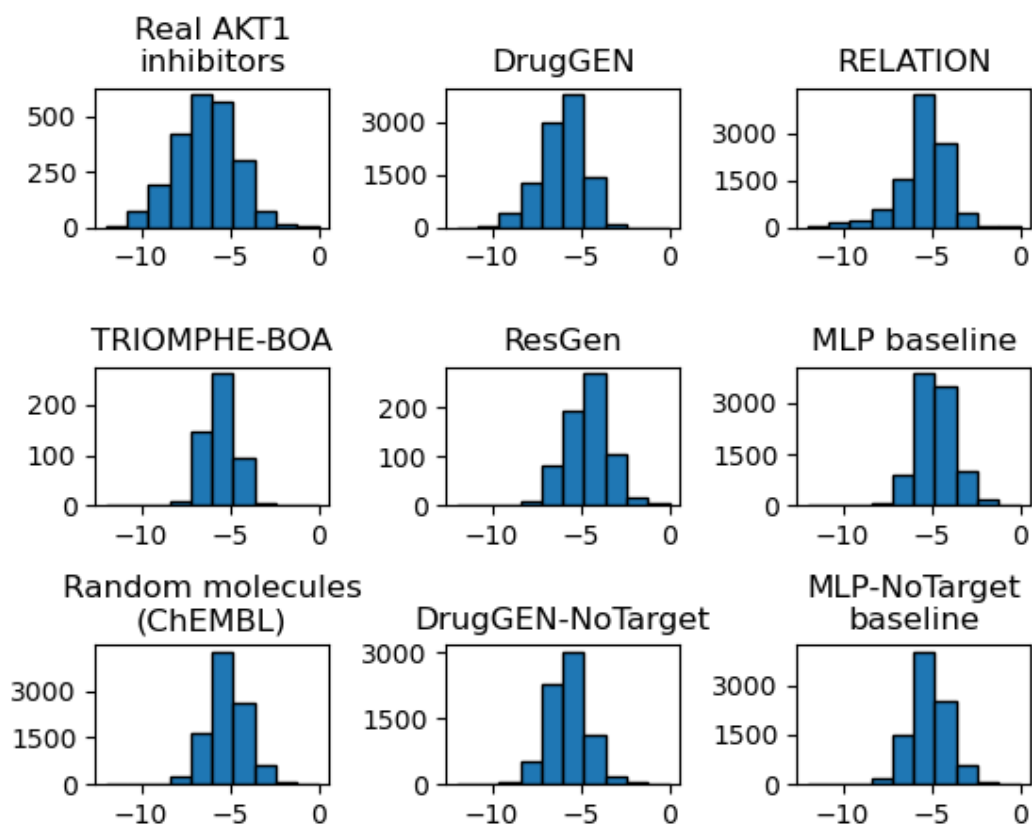


**Figure S3:** Docking score distributions of real AKT1 inhibitors, DrugGEN and DrugGEN-NoTarget models, MLP and MLP-NoTarget baseline models, ChEMBL molecules, and other target-centric molecule generation models, including RELATION, TRIOMPHE-BOA and ResGen.

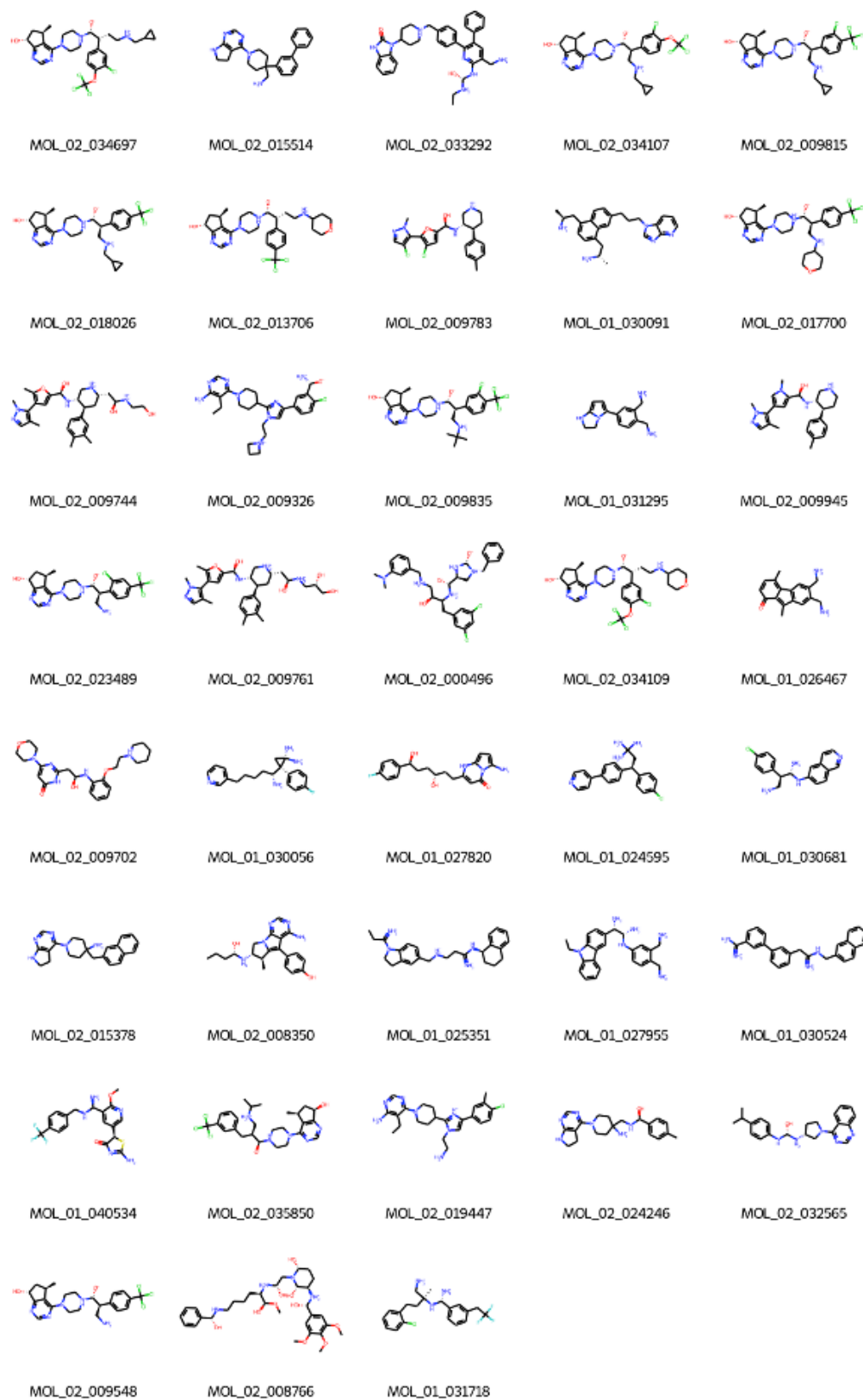


**Figure S4:** Thirty-eight molecules with predicted docking scores surpassing that of the native ligand capivasertib in the crystal complex structure of AKT1 “4GV1” (i.e., -9.517 kcal/mol).

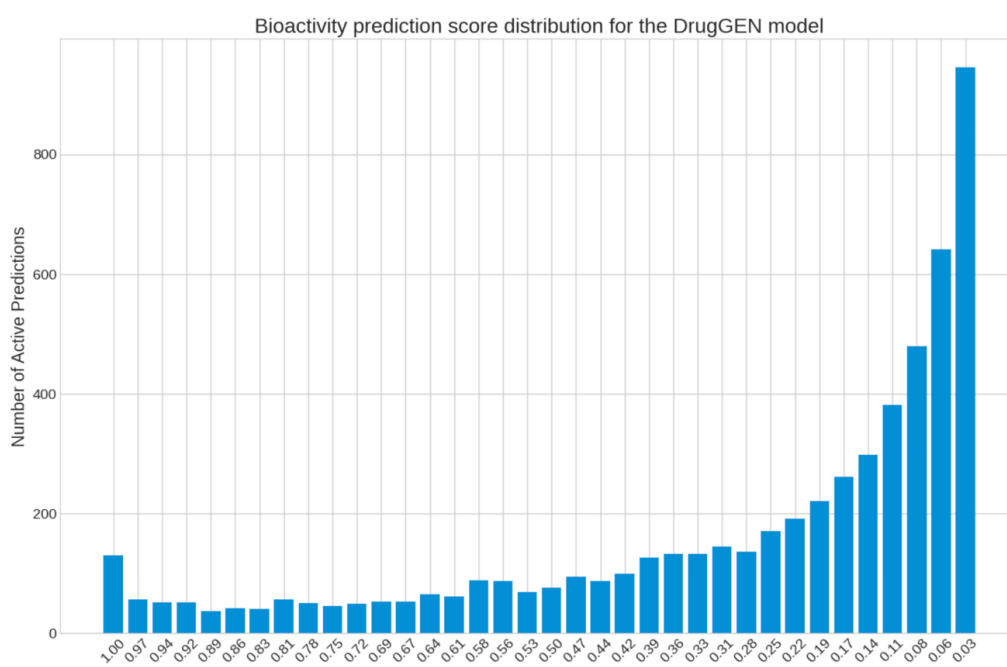


**Figure S5:** Drug-target interaction prediction confidence level histograms of 5,700 compounds generated by the DrugGEN model predicted to be active against the AKT1 protein. The results are produced by the DEEPScreen system (see “Methods” in the main text).

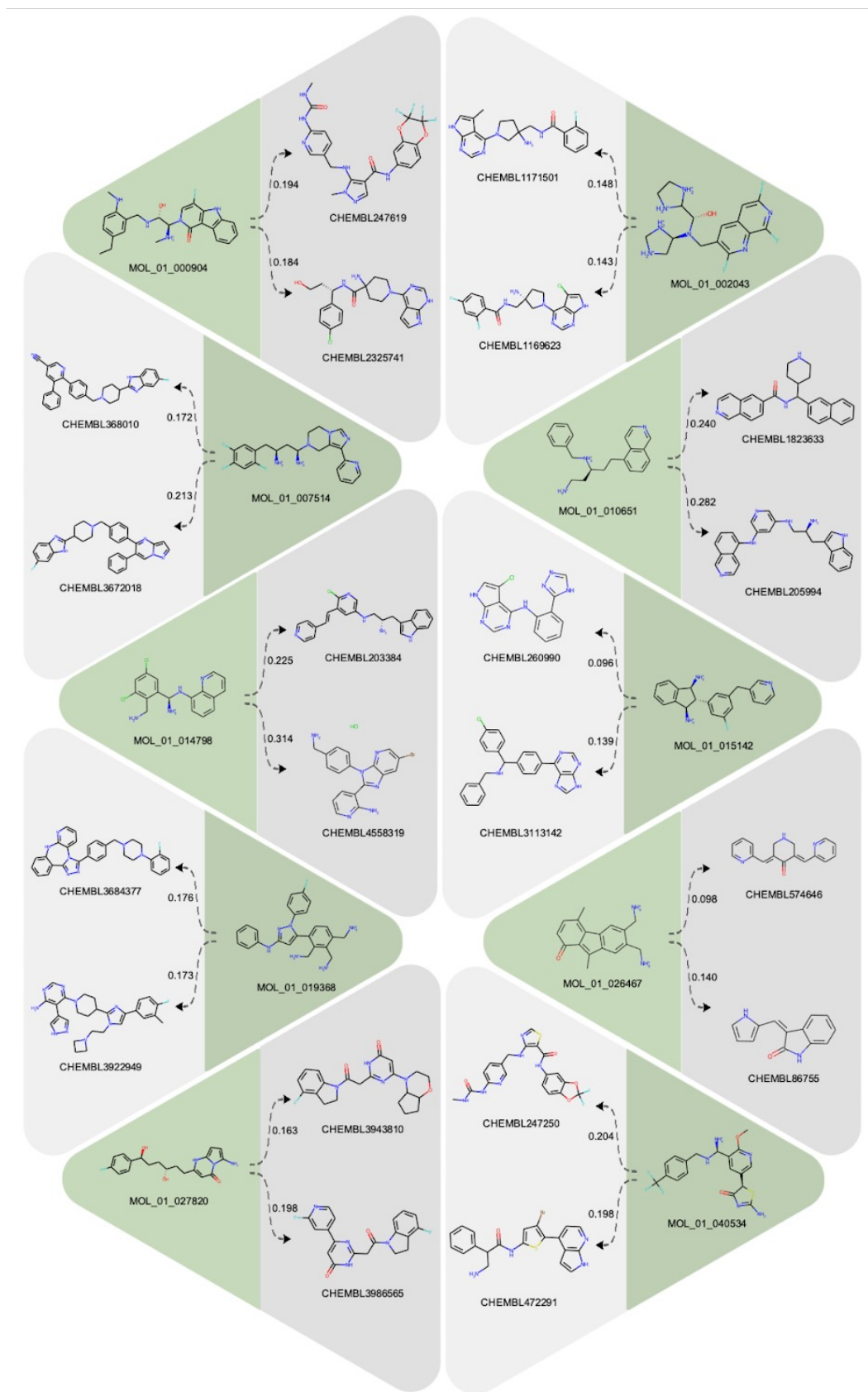


**Figure S6:** Ten randomly selected samples from 30 promising de novo molecules (displayed in Figure 3 of the main text) highlighted in green. Each DrugGEN molecule is shown with the most structurally similar two training dataset (ChEMBL) molecules (highlighted with grey). Real (ChEMBL) molecules are selected based on their substructure similarity to the de novo designs using the Tanimoto coefficient on MACCS fingerprints.

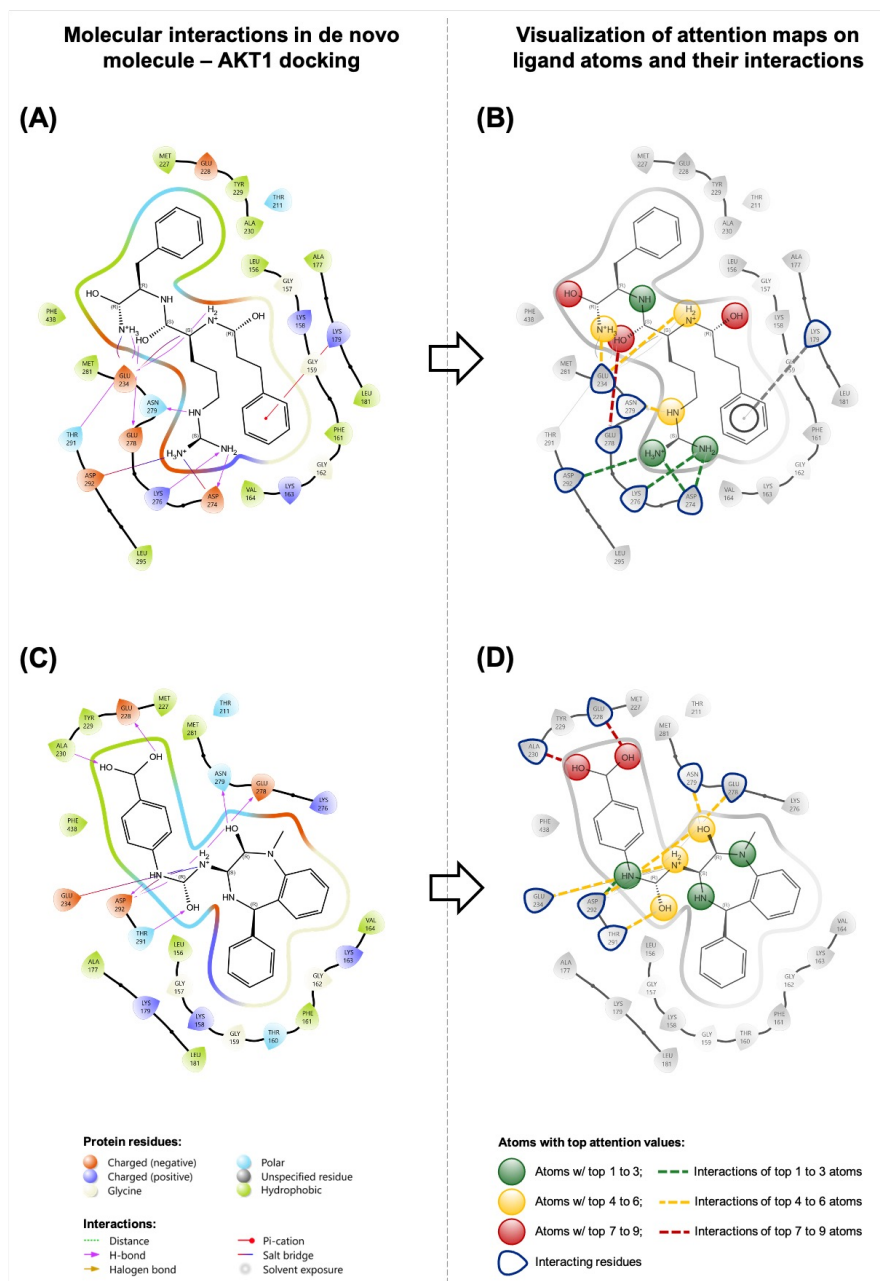


**Figure S7:** Visualisation of DrugGEN attention maps on two additional de novo molecules. The **left**-side column depicts protein-ligand interaction diagrams obtained from the molecular docking of DrugGEN’s three de novo molecules (in A, C and E) with the AKT1 protein structure (PDB id: “4GV1”). The docked ligands are located in the binding pocket, with interactions between residues and the ligand shown as lines, coloured by the interaction type. Protein residues are coloured according to their physicochemical properties. The **right**-side column depicts the attention maps of the same three de novo molecules (in B, D and F) retrieved from the graph transformer module of the DrugGEN generator network. Atoms that receive the highest attention scores are highlighted with colours (green: 1st, 2nd and 3rd atoms; yellow: 4th, 5th and 6th atoms; and red: 7th, 8th and 9th atoms with the highest attention scores). Atoms with lower attention scores are not coloured. In the right-side plots, receptor-ligand interactions (i.e., those obtained from the docking analysis) are represented by dashed lines in the attention-score-based colour of the molecule atom involved in the respective interaction. If an interacting atom could not be retrieved (i.e., the atom received a low attention score), its interaction is given in grey colour. **(A, B)** molecule id: *MOL\_02\_045598*, docking score: -9.055 kcal/mol, **(C, D)** molecule id: *MOL\_02\_000546*, docking score: -9.051 kcal/mol.

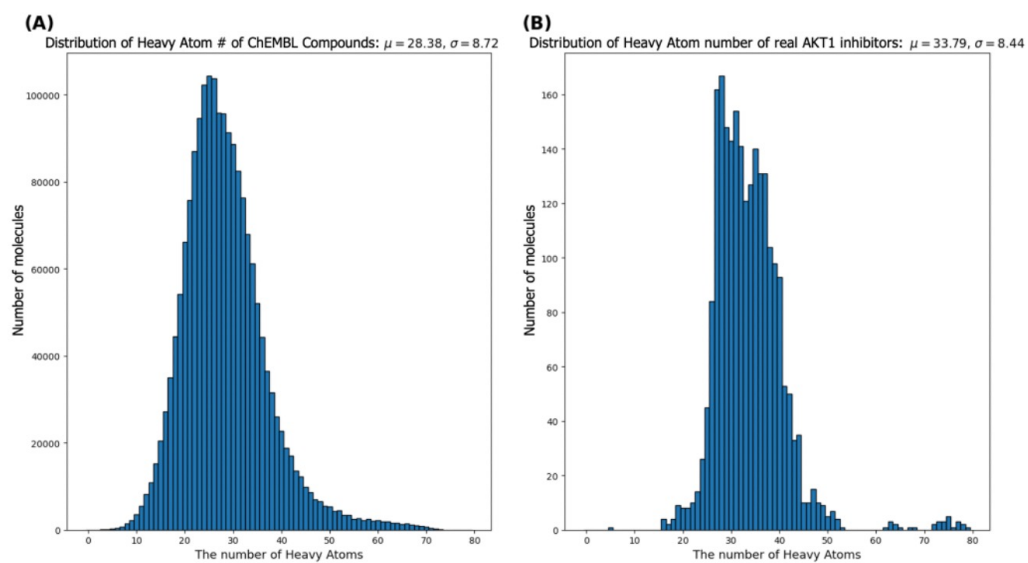


**Figure S8:** The heavy atom distribution histogram of (A) all of the small molecules in the ChEMBL database, and (B) recorded AKT1 binding small molecules in the ChEMBL database (v30).

## Supplementary Tables

**Table S1:** The number of transformer encoder blocks (depth) optimisation results for the DrugGEN model. Scores are provided in terms of percent-based performance loss (-) or gain (+) over the default model.

	1-Depth	2-Depth	4-Depth	6-Depth
Validity	-	-35%	-34%	-89%
Uniqueness	-	0%	-4%	-8%
Novelty	-	-2%	-3%	+9%